BARC/2013/E/003

BARC/2013/E/003

STEADY STATE AND STABILITY CHARACTERISTICS OF A SUPERCRITICAL PRESSURE NATURAL CIRCULATION LOOP (SPNCL) WITH CO_2

by

P.K. Vijayan, Manish Sharma and D.S. Pilkhwal
Reactor Engineering Division

2013

BARC/2013/E/003

BARC/2013/E/003

GOVERNMENT OF INDIA
ATOMIC ENERGY COMMISSION

STEADY STATE AND STABILITY CHARACTERISTICS OF A SUPERCRITICAL PRESSURE NATURAL CIRCULATION LOOP (SPNCL) WITH CO_2

by

P.K. Vijayan, Manish Sharma and D.S. Pilkhwal
Reactor Engineering Division

BHABHA ATOMIC RESEARCH CENTRE
MUMBAI, INDIA
2013

BIBLIOGRAPHIC DESCRIPTION SHEET FOR TECHNICAL REPORT
(as per IS : 9400 - 1980)

01	*Security classification :*	Unclassified
02	*Distribution :*	External
03	*Report status :*	New
04	*Series :*	BARC Exernal
05	*Report type :*	Technical Report
06	*Report No. :*	BARC/2013/E/003
07	*Part No. or Volume No. :*	
08	*Contract No. :*	
10	*Title and subtitle :*	Steady state and stability characteristics of a supercritical pressure natural circulation loop (SPNCL) with CO_2
11	*Collation :*	38 p., 33 figs., 3 tabs., 1 ill.
13	*Project No. :*	
20	*Personal author(s) :*	P.K. Vijayan; Manish Sharma; D.S. Pilkhwal
21	*Affiliation of author(s) :*	Reactor Engineering Division, Bhabha Atomic Research Centre, Mumbai
22	Corporate author(s) :	Bhabha Atomic Research Centre, Mumbai - 400 085
23	*Originating unit :*	Reactor Engineering Division, BARC, Mumbai
24	*Sponsor(s) Name :*	Department of Atomic Energy
	Type :	Government

Contd...

BARC/2013/E/003

30	*Date of submission :*	January 2013
31	*Publication/Issue date :*	February 2013
40	*Publisher/Distributor :*	Head, Scientific Information Resource Division, Bhabha Atomic Research Centre, Mumbai
42	*Form of distribution :*	Hard copy
50	*Language of text :*	English
51	*Language of summary :*	English, Hindi
52	*No. of references :*	34 refs.
53	*Gives data on :*	

60

Abstract : Supercritical pressure natural circulation experiments were carried out with CO_2 in a uniform diameter rectangular loop. Experimental data were generated on, steady state flow, heat transfer and stability under natural circulation conditions. The steady state flow rate data obtained were compared with the predictions of 1-D code NOLSTA which showed good agreement. The supercritical heat transfer coefficient data showed a peak around the pseudocritical point. The heat transfer coefficient data were compared with different correlations reported in the literature. Good agreement was obtained with the prediction of McAdams, Bishop, Jackson and Jackson Fewester correlations. Instability was observed in the loop in a narrow window around the pseudo critical region with low cooling water flow rate for the HHHC orientation. All other orientations of heater and cooler were found to be stable. The stability data were compared with the predictions of the nonlinear stability analysis code NOLSTA. The details of the experimental set-up, experiments carried out and the results of the analysis are presented in this report.

70 *Keywords/Descriptors :* STEADY FLOW; SUPERCRITICAL STATE; WATER COOLED REACTORS; CRITICAL PRESSURE; CRITICAL TEMPERATURE; REACTOR COOLING SYSTEMS; NATURAL CONVECTION; REACTOR STABILITY; BOUNDARY CONDITIONS;

71	*INIS Subject Category :*	S21
99	*Supplementary elements :*	

Abstract

Supercritical pressure natural circulation experiments were carried out with CO_2 in a uniform diameter rectangular loop. Experimental data were generated on, steady state flow, heat transfer and stability under natural circulation conditions. The steady state flow rate data obtained were compared with the predictions of 1-D code NOLSTA which showed good agreement. The supercritical heat transfer coefficient data showed a peak around the pseudocritical point. The heat transfer coefficient data were compared with different correlations reported in the literature. Good agreement was obtained with the prediction of Mcadms, Bishop, Jackson and Jackson Fewester correlations. Instability was observed in the loop in a narrow window around the pseudo critical region with low cooling water flow rate for the HHHC orientation. All other orientations of heater and cooler were found to be stable. The stability data were compared with the predictions of the nonlinear stability analysis code NOLSTA. The details of the experimental set-up, experiments carried out and the results of the analysis are presented in this report.

CONTENTS

List of tables

List of figures

1.0 INTRODUCTION

Thermodynamically supercritical fluids are one of the several coolant options being investigated currently for advanced nuclear reactors. Both supercritical CO_2 [1-2] and supercritical water [3-6] are candidate coolants for advanced reactors. The advantage of supercritical fluids is higher thermodynamic efficiency due to the larger operating temperature possible. Since boiling is avoided, the critical heat flux phenomenon is eliminated raising the possibility of higher power density. Besides, supercritical fluids like water can be directly sent to the turbine eliminating the requirement of steam generator, steam-water separator and dryer. Further, most supercritical reactor designs proposed are once-through type eliminating the need for pressurizer and reducing the number of components like pumps. In addition, components like the primary pumps are of significantly lower rating compared to their counterparts in the current LWRs of the same rating due to the significantly lower core flow rate resulting from the larger enthalpy rise across the core. The higher power density could significantly lower the core size. Also pressure retaining parts can be designed at lower temperatures compared to current reactor designs. The foregoing advantages suggest that the supercritical reactor could be far more competitive economically compared to the current LWRs.

However, supercritical fluids undergo significant property changes in the pseudo-critical region. For example, the density changes in supercritical reactors are comparable to or more than that in present day BWRs raising the possibility of density wave instability in these reactors. In view of this, several investigators have already looked at the instability of supercritical fluids [7-8]. A few investigations were also conducted with supercritical CO_2 which is a good simulant fluid for water [9-11]. Fluid-to-fluid modeling aspects have been studied by Marcel et al. [12] and found that a 77.5%/22.5% mixture of refrigerants R-32 & R-125 simulates the supercritical water (SCW) conditions in HPLWR (High Performance Light Water Reactor). They also found that supercritical CO_2 cannot accurately simulate the HPLWR conditions with water. A few studies have been made to extend the generalized dimensionless parameters applicable for stability analysis of two-phase flows to supercritical fluids [13-14]. Some of these studies were carried out in natural circulation systems [9-11 & 15] as it is also a possible option for supercritical reactors [16-17]. However, very few experimental studies are reported in the open literature. To our knowledge, the supercritical test data are reported in rectangular loops by Lomperski et al. [18] and Holman and Boggs [19] with supercritical CO_2 and Freon-12 respectively. Besides Yoshikawa et al. [20] studied the performance of a supercritical CO_2 natural circulation in a somewhat complex loop. In the context of the above an experimental investigation of the steady state and stability behavior has been carried out in a rectangular natural circulation loop with supercritical CO_2 as the working fluid and the results are presented here.

Apart from stability the heat transfer and pressure drop characteristics of supercritical fluids are important for design. Due to the large property variations in the pseudocritical region, traditional single-phase heat transfer correlations are not adequate to predict the heat transfer for supercritical fluids. Several investigators have also reported deterioration in heat transfer in the pseudocritical region similar to that observed in two-phase flows following the occurrence of CHF [21-22]. However, the reported degradation is marginal compared to that occurring post CHF conditions in two-phase flows. Investigations in rod bundles have not shown any degradation in heat transfer. Thus it is necessary to study the heat transfer behavior in supercritical systems which are also carried out in the present test facility.

2.0 THE EXPERIMENTAL LOOP

Fig.1 shows the schematic of the experimental loop. It is a uniform diameter rectangular loop made of 13.88 mm inside diameter stainless steel (SS-347) pipe with outside diameter of 21.34 mm. Standard 41.4 MPa (6000 lb) rating socket weld type elbows are used at the corners (see detail A in Fig. 1). The loop has two heater test sections and two cooler test sections so that the loop can be operated in any one of the four orientations such as Horizontal Heater Horizontal Cooler (HHHC), Horizontal Heater Vertical Cooler (HHVC), Vertical Heater Horizontal Cooler (VHHC) and Vertical Heater Vertical Cooler (VHVC). The heater was made by uniformly winding nichrome wire over a layer of fiber glass insulation. The cooler was tube-in-tube type with chilled water as the secondary coolant flowing in the annulus. The outer tube forming the annulus had 77.9 mm inside diameter and 88.9 mm outside diameter. The loop had a pressuriser connected to the bottom horizontal pipe which takes care of the thermal expansion besides accommodating the cover gas helium above the carbon dioxide. The safety devices of the loop (i.e. rupture discs RD-1 & RD-2) were installed on top of the pressuriser which also had provision for CO_2 & He filling. The entire loop was insulated with three inches of ceramic mat (k=0.06 W/m^2).

2.1 Instrumentation

The loop was instrumented with 44 calibrated K-type mineral insulated thermocouples (1 mm diameter) to measure the primary fluid, secondary fluid and heater outside wall temperatures. Primary fluid temperatures at each location was measured as the average value indicated by two thermocouples inserted diametrically opposite at r/2 (see detail-D in Fig. 1) from the inside wall whereas secondary fluid temperatures were measured by a single thermocouple located at the tube centre. This was adequate to obtain the average temperature as the temperature rise in the secondary fluid was small (< 4 ^{o}C). The thermocouples used to measure the heater outside wall temperature were installed flush with the outside surface. To enable this, a longitudinal slot of width equal to the diameter of the thermocouple was cut on the outside surface and the thermocouple was inserted in this groove and brazed. There were 12 thermocouples at six axial distances installed at diametrically opposite locations. The system pressure was measured with the help of two Kellar make pressure transducers located on the pressuriser as well as at the heater outlet. The pressure drop across the bottom horizontal tube and the level in the pressuriser were measured with the help of two differential pressure transmitters. The power of each heater was measured with a Wattmeter. The secondary flow rate was measured with the help of three parallel turbine flowmeters. All instruments were connected to a data logger with a user selectable scanning rate. For all the transient and stability tests the selected scanning rate was 1 second.

Fig. 1: Photograph of SPNCL

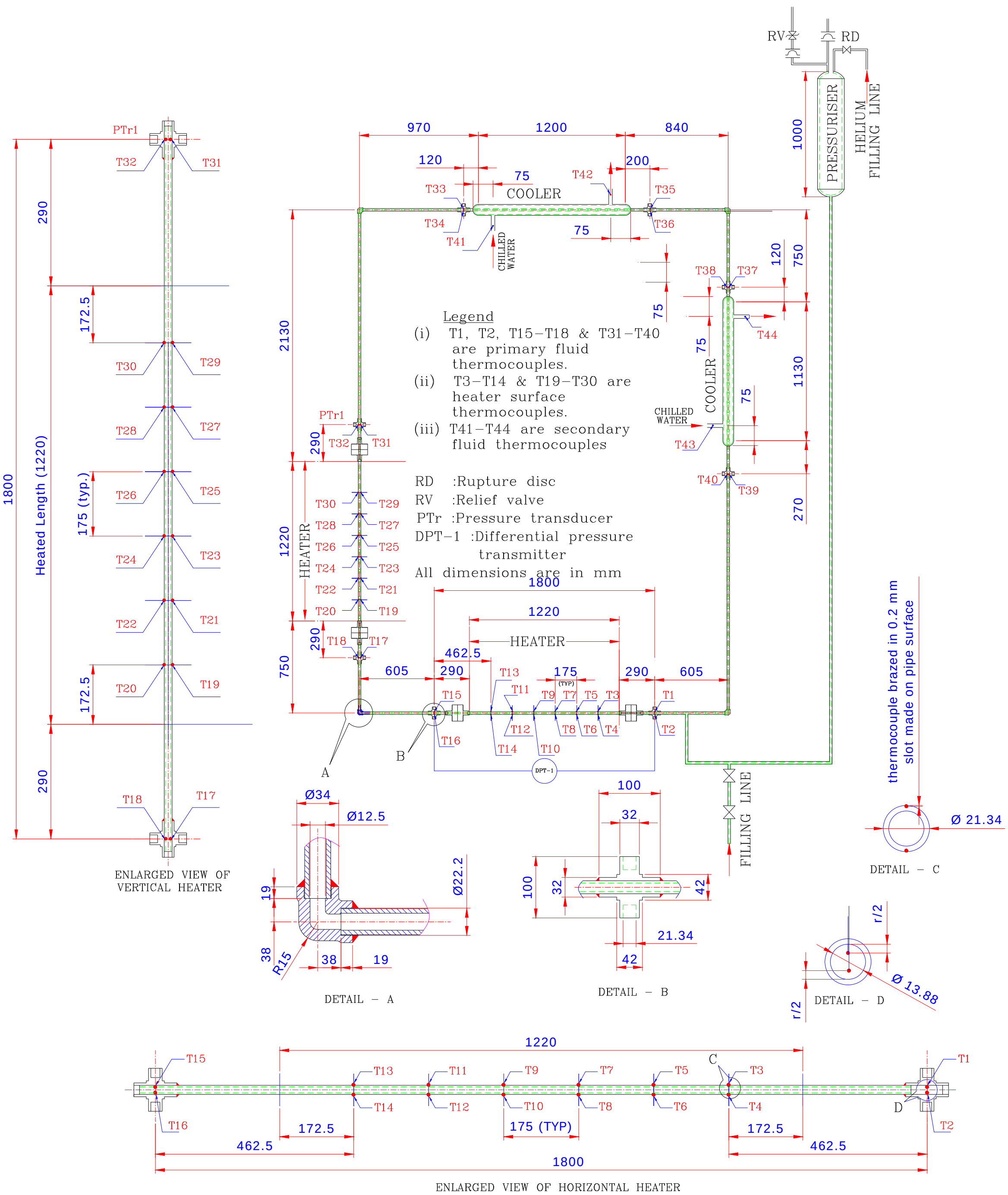

Fig. 1b:Schematic of SPNCL

Table-1: Fluctuations of measured parameters

Parameter	Fluctuation without power	Fluctuation under steady state natural circulation at 1400 W
Heater inlet temperature (^{o}C)	± 0.28	± 0.44
Heater outlet temperature (^{o}C)	± 0.44	± 0.43
Pressure (bar)	± 0.28	± 0.28
Pressure drop (mm WC)	± 0.21	± 0.21
Secondary inlet temperature (^{o}C)	± 0.1	± 0.07
Secondary outlet temperature (^{o}C)	± 0.35	± 0.47

The accuracy of the thermocouples were within ± 1.5 ^{0}C. The accuracy of the pressure and differential pressure measurements were respectively ± 0.3 bar and ± 0.18 mm. The accuracy of the secondary flow as well as power measurement is ± 0.5 % of the reading. In addition, typical fluctuations of each instrument were also recorded during steady state with and without power (stagnant initial conditions). As seen from Table-1, there is hardly any difference in the fluctuations with and without power.

2.2 Shakedown Tests

The purpose of the shakedown tests was to generate heat loss and pressure drop characteristics of the loop. The pressure drop characterization tests were carried out under forced flow conditions with the help of a pump in a separate facility using the same bottom horizontal pipe and one of the elbows installed horizontally. Apart from flow rate and pressure drop, the temperature was also measured at different flow rates in this facility. From the measured pressure drop across the bottom horizontal pipe and the flow rate, the friction factor for the pipe was estimated by the following equation.

$$f = \frac{2D\rho A^2 \Delta p_m}{L w_m^2} \tag{1}$$

The estimated friction factor is plotted in Fig. 2. The measured friction factor was somewhat larger than that for smooth pipes due to the use of commercial pipes. The correlation fitted to the friction factor data is also shown in Fig. 2. From the measured pressure drop across the elbow and the flow rate, the loss coefficient was estimated as below.

$$K = \frac{2\rho A^2 \Delta p_m}{w_m^2} \tag{2}$$

The loss coefficient data generated at forced flow condition is plotted in Fig. 3. A correlation was also fitted to the data. The loss coefficient was found to be constant at 0.55 for Reynolds numbers greater than 45,000.

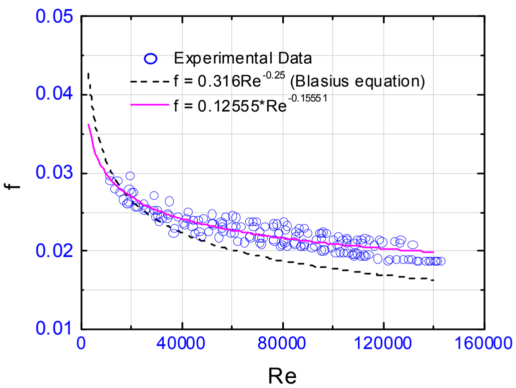

Fig. 2: Friction factor data for the tube used in the construction of the loop

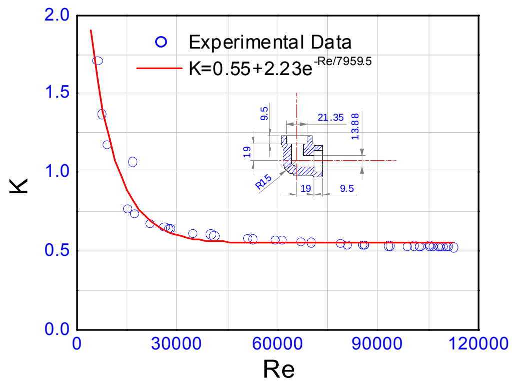

Fig. 3: Loss coefficient data for the 90° elbow used in the loop

To test the adequacy of the loop instrumentation for estimating the heat transfer coefficient and loop mass flow rate as well as to estimate the heat losses, natural circulation experiments were carried out at various powers with water at subcritical conditions. These experiments were carried out at a system pressure of 30 bar for all the four orientations of the heater and cooler. The natural circulation mass flow rate was estimated by a heat balance across the heater as shown below.

$$\dot{w} = \frac{Q_h}{Cp\left(T_{ho} - T_{hi}\right)} \tag{3}$$

The estimated mass flow rates under subcritical single-phase natural circulation condition are compared in Fig. 4 with that estimated theoretically using the following equation.

$$w = \left[\frac{2D^{1+b}\rho^2 \beta g A^{2-b} Q_h \Delta z}{pCp\mu^b}\right]^{\frac{1}{3-b}} \tag{4}$$

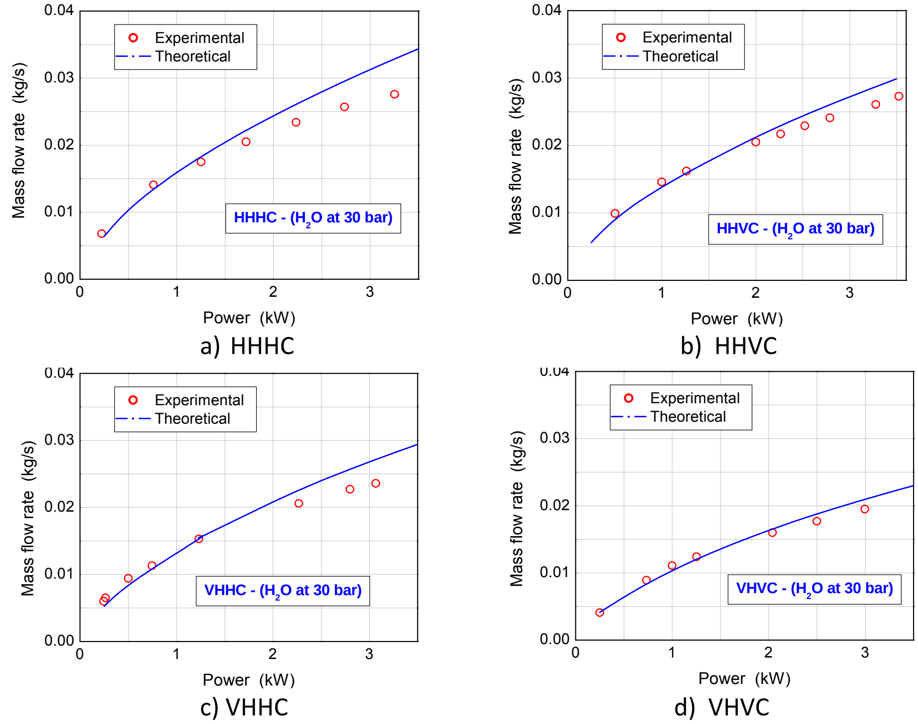

Fig.4: Comparison of measured and predicted subcritical natural circulation flow rate for various orientations

Subsequently, the data are also compared with the dimensionless correlation proposed by Swapnalee & Vijayan [23] in Fig. 5. In either case good agreement is obtained between theoretical and experimental values. To estimate the heat transfer coefficient, first the local inlet wall temperature was estimated from the measured local heater outer surface temperature as below.

$$T_{wi} = T_{wo} - \frac{Q_h \ln\left(\frac{r_o}{r_i}\right)}{2\pi L k} \tag{5}$$

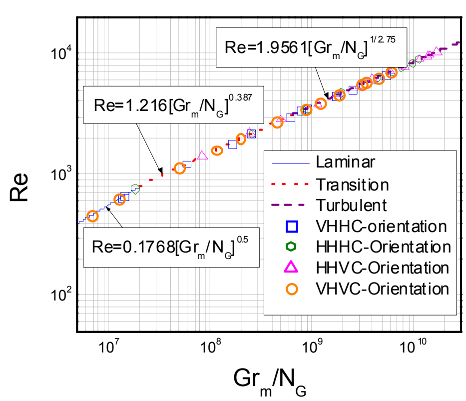

Fig. 5: Measured and predicted flow rate for subcritical water

Then the local bulk fluid temperature was estimated using the measured heater inlet and outlet temperatures using the following equation.

$$T_b = T_{hi} + \frac{x\left(T_{ho} - T_{hi}\right)}{L_h} \tag{6}$$

Where x is the distance from the inlet of heated section. Then the local heat transfer coefficient was estimated as below.

$$h = \frac{q_h}{\left(T_{wi} - T_b\right)} \tag{7}$$

Six such local heat transfer coefficients were estimated corresponding to the thermocouple locations (along the length of each heater) and using these values an average heat transfer coefficient was estimated and plotted as shown in Fig. 6. The heat transfer coefficient predicted by the Dittus-Boelter correlation is also shown in these figures. The total estimated heat loss fraction as a function of the heater power is plotted in Fig. 7. The heat loss fraction is estimated using the measured Q_h as

$$F = \frac{Q_h - Q_c}{Q_h} = \frac{\Delta T_h - \Delta T_c}{\Delta T_h} \tag{8}$$

The heat rejected at the cooler, Q_c, is estimated using the measured cooler inlet and outlet primary temperatures as below.

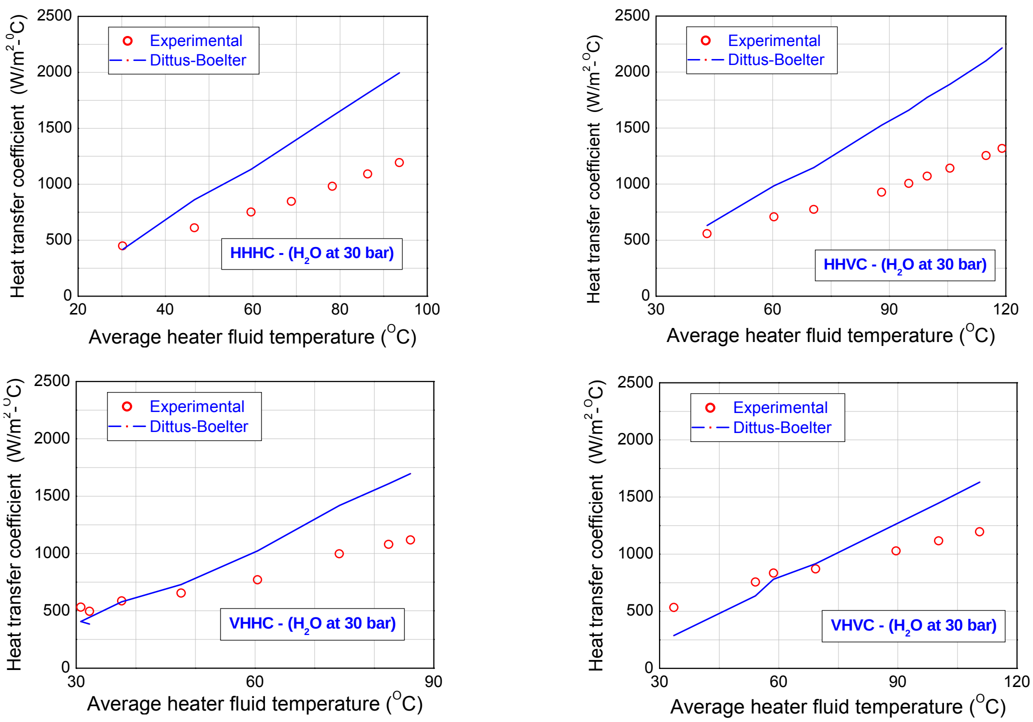

Fig. 6: Estimated subcritical heat transfer coefficient for different orientations

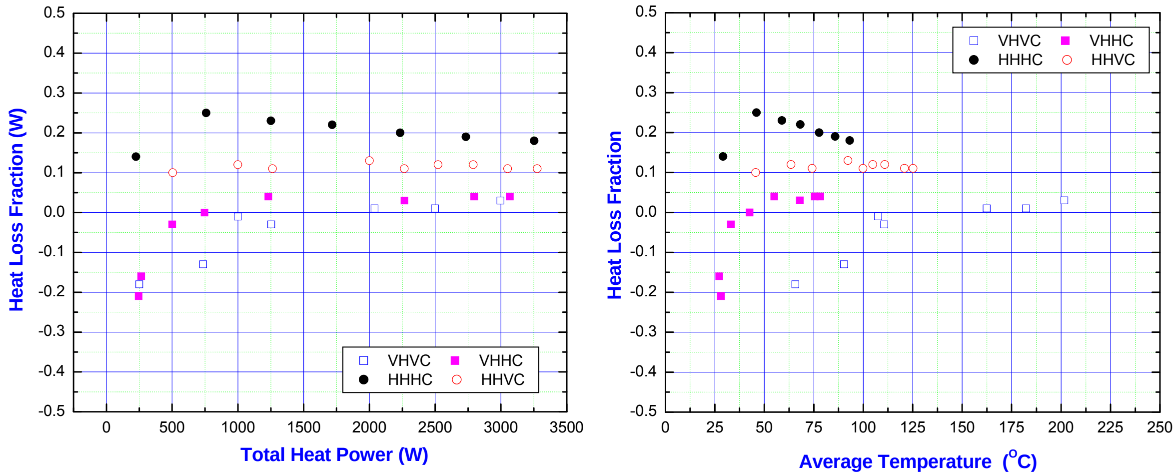

(a) **(b)**

Fig. 7: Estimated heat loss fraction for various orientations during NC experiments with

$$Q_c = wCp(T_{ci} - T_{co}) \tag{9}$$

Where w is estimated using Eq. (3). Since the ambient temperature was significantly high (30±2 °C) compared to the chilled water coolant temperature (9.8±1.6 °C), in certain low power cases, heat gain was observed instead of loss. As seen from Fig. 7b, the heat loss for different orientations are different due to the differences in the hot and cold leg lengths.

2.3 Operation with Supercritical CO_2

Before operation with supercritical CO_2, the loop was flushed repeatedly with CO_2 at low pressure including all impulse, drain and vent lines. Subsequently the loop was filled with CO_2 up to 50 bar pressure and the chilled water coolant was valved in. This caused condensation of CO_2 and hence a decrease in loop pressure. The pressure decrease was compensated by admitting additional CO_2 from the cylinder and again allowed sufficient time for condensation. The process of filling and condensation was continued till there was no decrease in pressure. At this point the loop pressure was increased to the required value with the help of a helium gas cylinder. Once the required supercritical pressure was achieved, the helium cylinder was isolated. Sufficient time was allowed to reach a steady state. However, it was found difficult to attain completely stagnant conditions with uniform temperature throughout the loop as the higher ambient temperature allowed small amount of heat absorption through the insulation into the loop which was rejected at the cooler causing a small circulation rate. Once a steady state was achieved, the heater power was switched on and adjusted to the required value. Sufficient time was allowed to achieve the steady state. Once the steady state is achieved, power was increased and again sufficient time was provided to achieve the steady state. In case the system pressure increases beyond the set value by 1 bar, a little helium was vented out to bring back the pressure to the original value. Similarly during power decrease if the pressure decreases below the set point by one bar, then the loop was pressurized by admitting additional helium into the pressurizer. The experiments were repeated for different pressures and different chilled water flow rates. Subsequently the experiments were performed for different orientations of the heater and cooler.

3.0 STEADY STATE DATA

Steady state data on natural circulation flow rate and heat transfer were generated with supercritical CO_2 for various orientations of the source and sink. The range of parameters of all the steady state data is

Orientations studied : HHHC, HHVC, VHHC and VHVC
Pressure : 8-9.1 MPa
Power : 0.1-2.4 kW
Cold leg temperature : 17.5-57.7 ^oC
Hot leg temperature : 19.3-95.9 ^oC
Coolant flow rate : 29.6-56 lpm (liters per minute)
Coolant inlet temperature : 8.2-11.4 ^oC
Coolant outlet temperature : 9.0-12.5 ^oC

3.1 Steady State Natural circulation Flow Rate with Supercritical CO_2

Steady state data for the different heater-cooler orientations (i.e. HHHC, HHVC, VHHC & VHVC) were generated in the loop. Appendix-1 shows the complete set of steady state data generated. Table-2 shows the range of parameters for steady state data for each orientation. The steady state mass flow rate for the experimental conditions were estimated using the measured heater power and the enthalpy rise across the heater as

$$w = \frac{Q_h}{i_{ho} - i_{hi}} \quad (10)$$

Table-2: Range of parameters for steady state tests with supercritical CO_2

Orientation	Power (kW)	Loop conditions			Secondary coolant conditions		
		Pressure (MPa)	Temperature (^oC)		Flow rate (lpm)	Temperature (^oC)	
			Cold leg	Hot leg		Inlet	Outlet
HHHC	0.19-2.4	8.5-9.2	17.7-57.7	20.5-95.9	29.6-37	8.7-10.2	9.5-11.7
HHVC	0.3-2.2	8.5-8.8	20.2-49.3	24.2-93.1	33.5-34.8	8.2-9.3	9-10.4
VHHC	0.14-2.4	9-9.26	17.5-49.5	19.6-73.9	31.6-38	8.5-11.4	9.7-12.5
VHVC	0.1-2.0	8.1-9.1	17.5-41.3	19.3-66.8	36.2-56	8.6-9.5	8.8-9.7

The enthalpies at the heater inlet and outlet were estimated using the corresponding measured temperatures and system pressure. This is a better approach to estimate the experimental flow rate since the specific heat variation is significant. The flow rates so estimated were compared with the predictions of the in-house developed computer code NOLSTA [24] and the results are presented in Fig. 8a & b. Figure 8a shows the data for three different orientations for which data were available at 8.6 MPa. For the VHHC orientation data were available only for 9.1 MPa. The data for VHHC and HHHC orientations are compared with NOLSTA predictions in Fig. 8b. The data are found to be in close agreement with the code predictions.

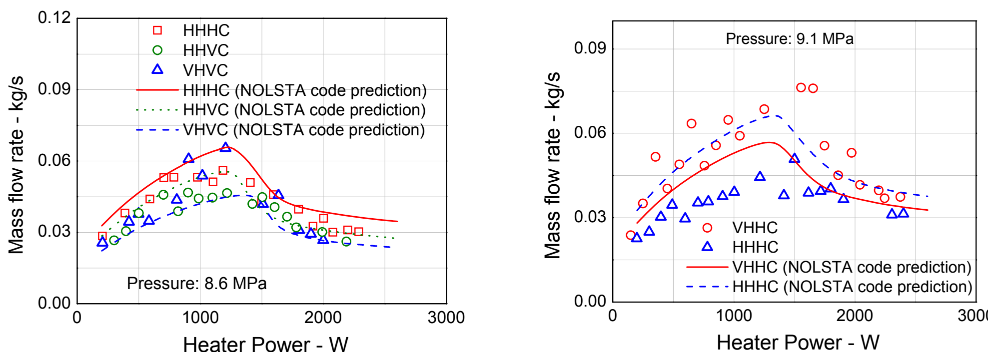

(a) Steady state flow rate at 8.6 MPa **(b) Steady state flow rate at 9.1 MPa**

Fig. 8: Measured and predicted steady state flow rate for various orientations

3.2 Effect of pressure

The data on the effect of pressure on the steady state flow rate are presented in Fig. 9 along with the predictions by the NOLSTA code. Subsequently, all the data are presented in dimensionless form in Fig. 10. The dimensionless flow correlations obtained using the Blassius and the experimental friction factor (see Fig. 2) correlations are also plotted in Fig. 10. The data are found to be in reasonable agreement with the experimental friction factor correlation.

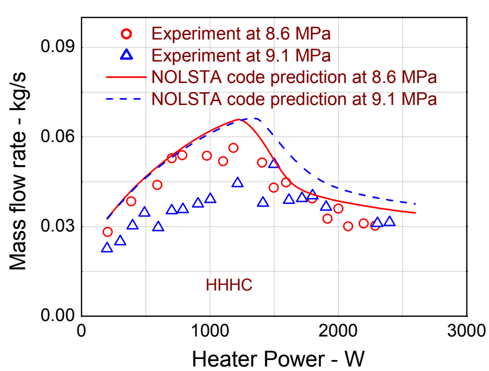

Fig. 9: Effect of pressure on the steady state

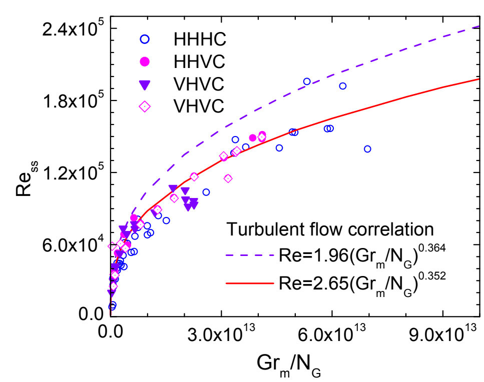

Fig. 10: Steady state flow for various orientations

3.3 Heat Transfer Coefficient

The heat transfer coefficient was estimated by the same procedure as given in section 2.2 from the measured outside wall temperature and the fluid temperature. The range of parameters for heat transfer data are given below

Reynolds number	: 2.5×10^4-3.1×10^5
Prandtl number	: 1.1-6.5
Nusselt number	: 90-800
Heat flux	: 2.5-50 kW/(m^{2}K)
Mass flux	: 140-500 kg/(m^{2}s)
Wall temperature	: 15 - 95 ^{o}C

The local heat transfer coefficients were averaged over the length and the average value was then compared with the predictions of different correlations reported in literature. Fig. 11 and 12 show the measured heat transfer coefficient in the horizontal and vertical heated sections compared with different correlations. As seen from the figures, Bishop [26], Jackson-Fewster [28], McAdams [30] and Jackson [31] correlations represent the data well. Comparing the heat transfer coefficient data given in figures 11 and 12 with that for subcritical flow given in Fig.6, it is found that there is a peak in supercritical data which is missing in the subcritical data.

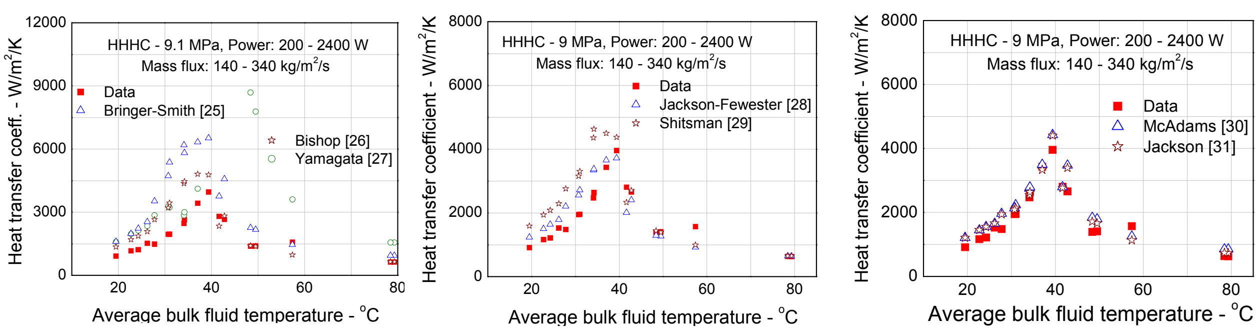

Fig. 11: Heat transfer coefficient in horizontal heater compared with various correlations

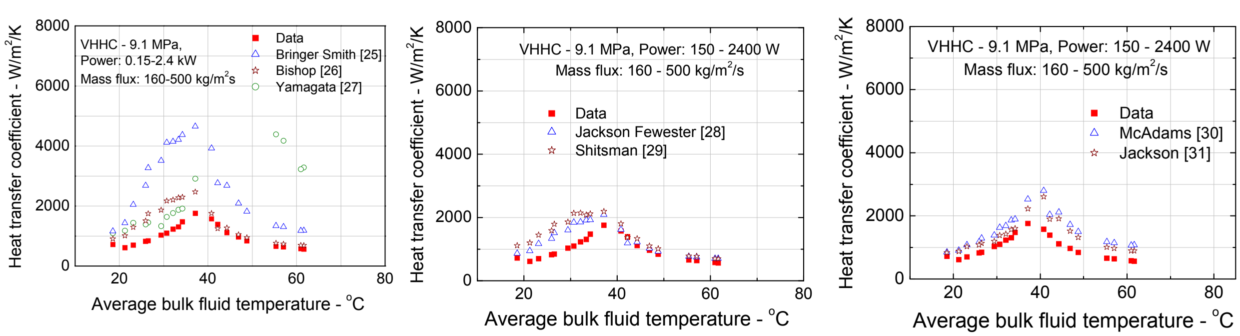

Fig. 12: Heat transfer coefficient in vertical heater compared with various correlations

4.0 STABILITY DATA

Instability was observed only for the HHHC orientation. All other orientations were fully stable. Even for the HHHC orientation, both the subcritical and the supercritical regions beyond the pseudo-critical region were found to be mostly stable. Instability was observed only for a narrow window in the pseudo-critical region at low secondary coolant flow rates (25 lpm and less).

4.1 Instability Experiments

Instability was observed during the following experiments:

a) Start-up from rest
b) Power raised or lowered from a stable steady state
c) Large power decrease from a stable steady state

It may be noted that although instability was observed in all the above categories, thresholds of instability could not be established precisely in all cases. Table-3 lists all the instability data that was generated in the facility. As seen from the table most instability data are for 10 or 15 lpm.

4.2.1 Start-up from rest

These tests were performed as described in section 2.3. After valving in the chilled water flow nearly 3-4 hours were provided to achieve steady state. Since the ambient temperature (28-32 ^{o}C) was much above the coolant temperature (8.2-11.4 ^{o}C), complete stagnant conditions could not be achieved as explained in section 2.3. Typical instabilities observed for start-up from rest are shown in Fig. 13. At 10 lpm flow, stable start-up is not observed in the clockwise flow direction for powers greater than 200 W. Start-up tests were not performed below this power. However, analysis shows stable start-up at very low power. On the other hand if flow initiated in the counter-clockwise direction, it was found to be stable. Note that the loop is not completely symmetric (see Fig. 1).

4.2.2 Power raised or lowered from stable steady state

In this case, starting from a stable steady state the power is increased or decreased in small steps. These experiments were carried out at different pressures and secondary flow rates. Table-3 shows a summary of the tests done.

Typical instability observed at 9.1 MPa at various powers is shown in Fig. 14, 15 and 16 respectively for different secondary flow rates of 10, 15 and 20 lpm. In all cases, the instability develops by the oscillation growth mechanism as proposed by Welander [32]. Instability was also observed at other pressures as shown in Fig. 17.

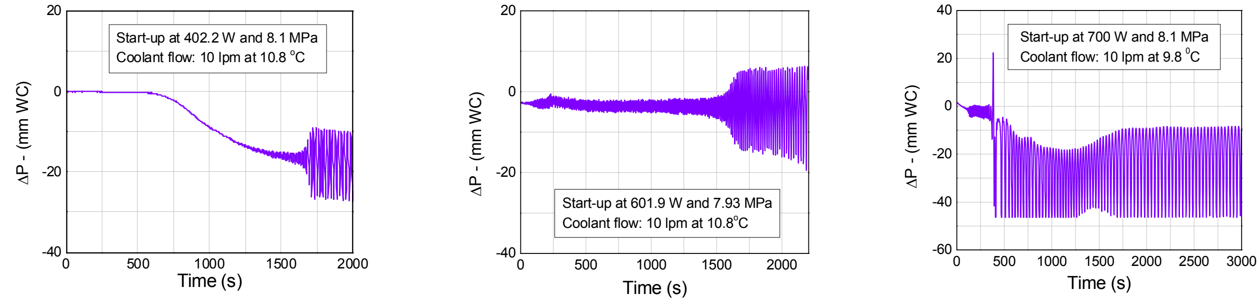

a) Unstable start-up at 402.2 W **c) Unstable start-up at 601.9 W** **d) Unstable start-up at 700 W**

Fig. 13: Start-up from rest at different powers

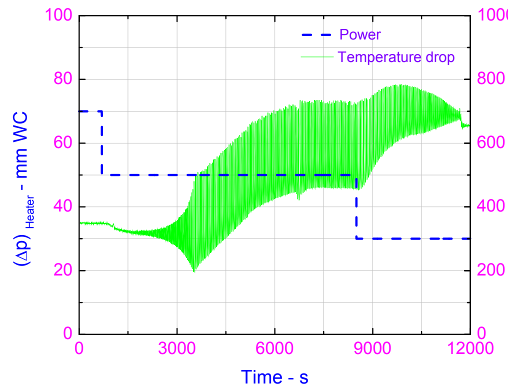

Fig. 14: Typical instability observed at 500 W and 9.1 MPa with 10 lpm secondary flow

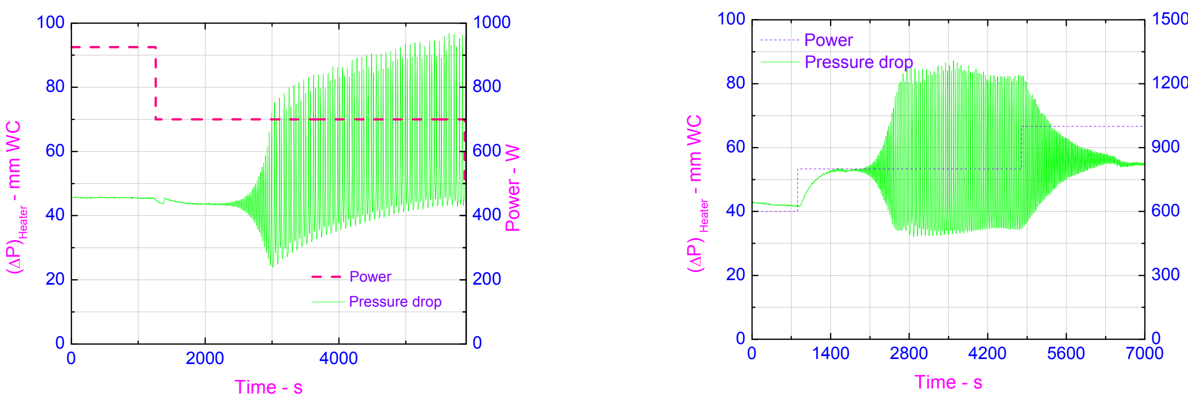

a) Instability at 700 W **b) Instability at 800 W**

Fig. 15: Instability observed at different powers at 9.1 MPa and 15 lpm secondary flow

Table-3: Summary of instability data

Sl. No.	Gauge pressure (MPa)	Power (W)	Secondary flow		Stability data file name*	Remark
			Flow rate (LPM)	Coolant inlet temp. (^{O}C)		
1	9.0	500	10.1	9.8	Stab_90_500_10.1_9.8.xls	Power decreased from 700 W to 500 W
2	9.0	700	15.5	9.8	Stab_90_700_15.5_9.8.xls	Power decreased from 925 W to 700 W
3	9.0	800	15.0	9.8	Stab_90_800_15_9.8.xls	Power increased from 600 W to 800 W
4	8.0	700	10.0	9.8	Stab_80_700_10_9.8.xls	Start up from rest at 700 W
5	7.6	300	10.0	9.1	Stab_76_300_10_9.1.xls	Power decreased from 1900 W to 300 W
6	8.1	300	10.1	9.2	Stab_80_300_10.1_9.2.xls	Power decreased from 1700 W to 300 W
7	8.1	400	10.0	10.8	Stab_81_400_10_10.8.xls	Start up from rest at 400 W
8	7.9	601	10.0	10.8	Stab_79_601_10_10.8.xls	Start up from rest at 601 W
9	8.1	1000	10.1	9.2	Stab_81_1000_10.1_9.2.xls	Power increased from 600 W to 1000 W
10	9.1	400	15.0	9.9	Stab_91_400_15_9.9.xls	Start up from rest at 400 W
11	9.1	300	20.0	9.5	Stab_91_300_20_9.5.xls	Power decreased from 1700 W to 300 W to 100 W
12	7.9	300	10.0	10.1	Stab_79_300_10_10.1.xls	Power decreased from 1500 W to 300 W

* The stability file names are given in such a way that they represent the operating conditions. For example in case of the first file, **Stab_90_500_10.1_9.8.xls**: 90 represents pressure in bar,
500 represnts power in W,
10.1 represent the coolant flow rate in LPM,
9.8 represent coolant inlet temperature in ^{O}C.

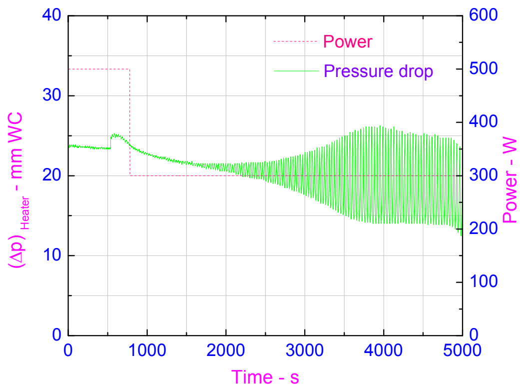

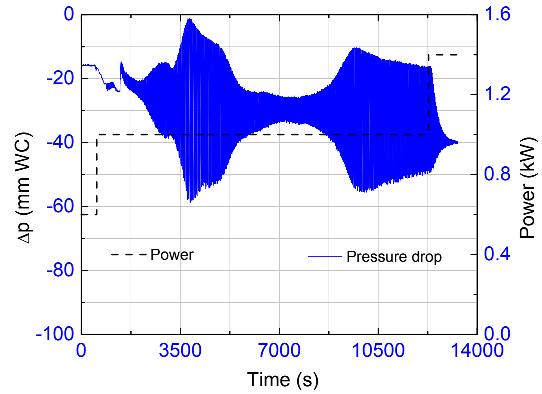

Fig. 16: Typical instability observed at 300 W and 9.1 MPa with 20 lpm secondary flow

Fig. 17: Typical instability observed at 1000 W and 8.1 MPa with 10 lpm secondary flow

4.2.3 Large power decrease from stable steady state

Three tests are listed under this category in table-3. In all cases the final power was the same and the initial power was different. Further the initial condition was stable and the final condition was unstable for all the cases (see Fig. 18).

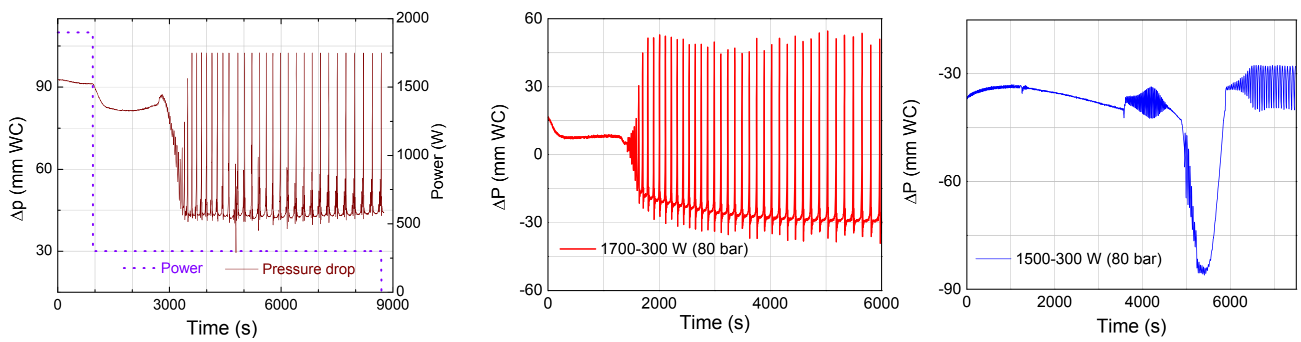

a) From 1900 W to 300 W **b) From 1700 W to 300 W** **c) From 1500 W to 300 W**

Fig. 18: Large power decrease from different initial powers

4.3 General Characteristics of the observed instability

The amount of instability data generated in the present test facility is clearly inadequate compared to the extensive instability data that exists for single-phase and two-phase loops. The data generated is also inadequate to confirm certain characteristics of the instability like hysteresis though its existence is suspected. Further, the instability thresholds have not been successfully identified. Nevertheless several interesting characteristics have been revealed by the limited unstable data generated in the facility as brought out below.

4.3.1 Oscillatory Behaviour of Heater Inlet and Outlet temperatures

The minimum and maximum of the observed heater inlet and outlet temperature oscillations for all the instability data at 8.1 and 9.1 MPa are shown in Fig. 19. Except for the start-up at 400 W, all other instability data is found to be either in the pseudocritical region or close to it. Thus it appears that operation in or around the pseudocritical region is prone to instability for supercritical fluids. However, the start-up instability is not necessarily a characteristic of supercritical fluids. Instability during start-up has also been observed earlier for single-phase natural circulation loops [33]. Thus apart from the instability around the pseudocritical region, SPNCLs are also susceptible to other instability mechanisms of natural circulation.

Another interesting feature of the oscillations is that the inlet temperature remains almost constant and only outlet temperature is oscillating (see Fig. 20). This, however, is not the case with the instability observed with large power decrease as well as start-up (see also Fig. 20d).

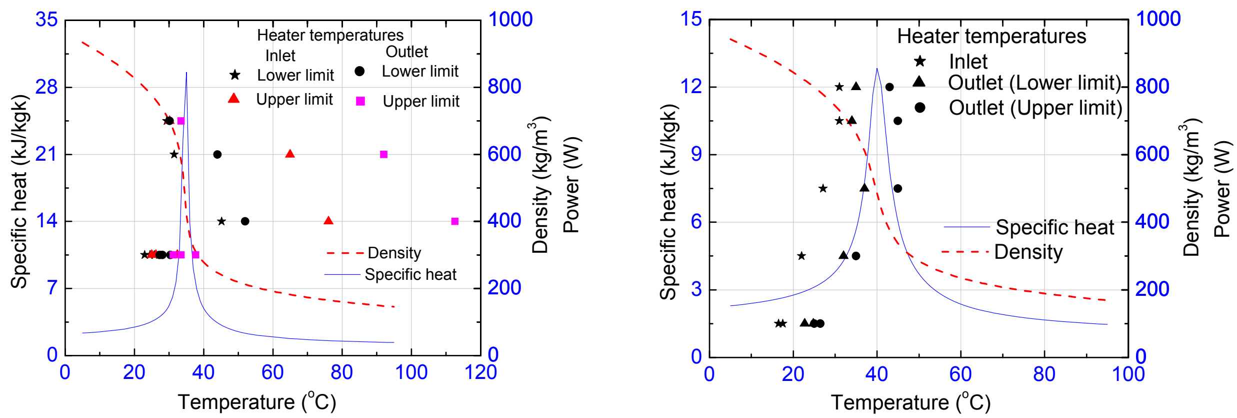

a) Data at 8.1 MPa **b) Data at 9.1 MPa**

Fig. 19: Inlet and outlet temperatures of the instability data at different pressures

4.3.2 Time Series and Phase Plots

Analyses of the test data neglecting the initial transients often reveal many interesting characteristics of the instability. Figures 21 to 23 show the time series of measured Δp (pressure drop across the bottom horizontal pipe), T_{hi} & T_{ho} (inlet and outlet temperatures of the heater) and the ΔT_h (temperature rise across the heater) for one thousand seconds after neglecting the initial transients. As can be seen, the phase plot (shown for only one cycle) shows a simple closed curve for the test data at 500 W (see Fig. 21d) which is markedly different from that shown in figures 22d and 23d. From the time series given in Fig. 21 and 22, it is easily seen that a near period doubling occurs between 500 W and 700 W. In general, the period is expected to decrease with increase in power if the oscillatory mode remains the same. Switching of the oscillatory mode as shown by the phase plots results in sudden period change. Periodic oscillations depict a single closed phase plot. Both the oscillatory modes characterized by the phase plots in Fig. 21 and 22 are only nearly periodic as shown by the long duration phase plots in Fig. 24. Also, the shape of the phase plots depends on the parameter spaces chosen (See Fig. 25).

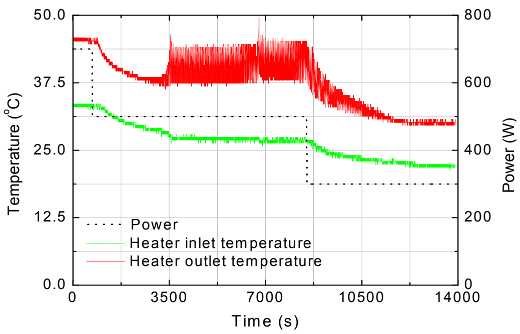

a) Temperature transient for test in Fig. 14

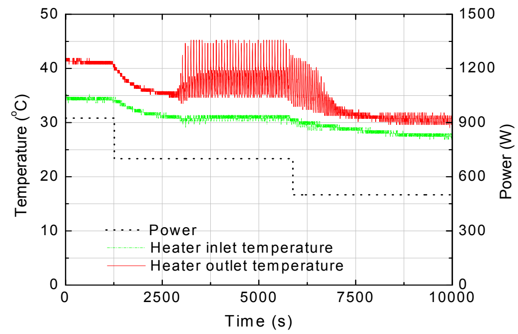

b) Temperature transient for test in

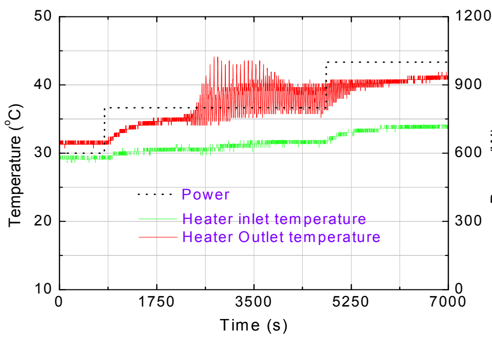

c) Temperature transient for test in Fig. 15b

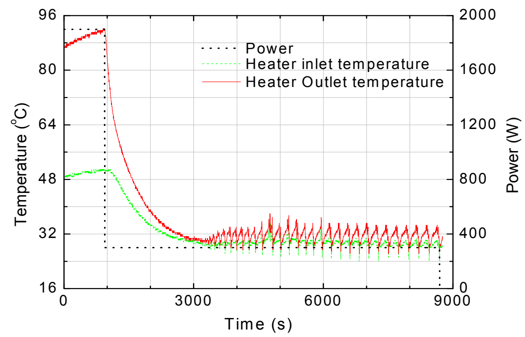

d) Temperature transient for test in Fig. 18a

Fig. 20: Typical inlet and outlet temperature oscillations for instability at different powers

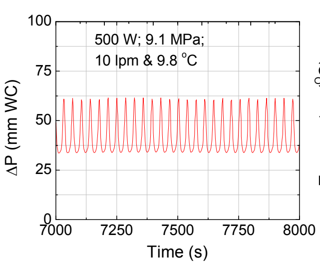

(a) Δp

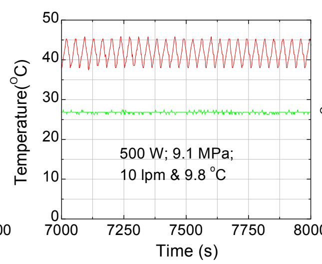

(b) T_{hi} and T_{ho}

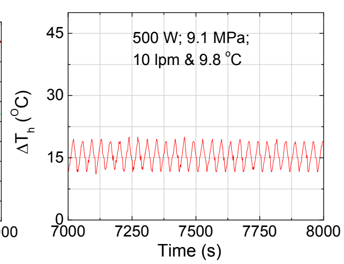

(c) ΔT_h

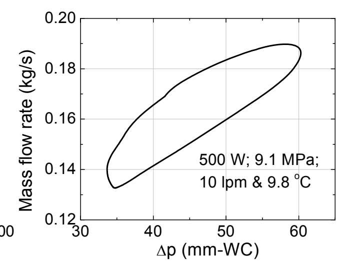

(d) Phase plot

Fig. 21: Time series and phase plot for the instability shown in Fig. 14

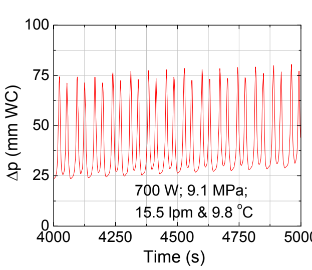

(a) Δp

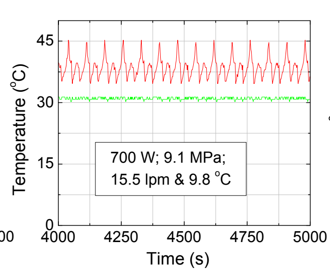

(b) T_{hi} and T_{ho}

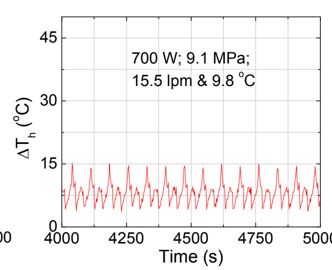

(c) ΔT_h

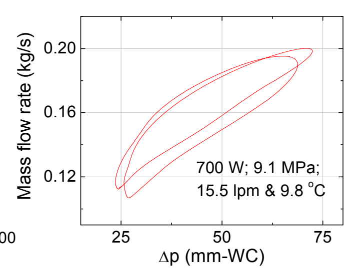

(d) Phase plot

Fig. 22: Time series and phase plot for the instability shown in Fig. 15a

5.0 STABILITY ANALYSIS

Nonlinear stability analysis code (NOLSTA) has been used for analysis of SPNCL with both open and closed loop boundary conditions. The formulations and the dicretisation scheme are explained in detail in Sharma et al [24].

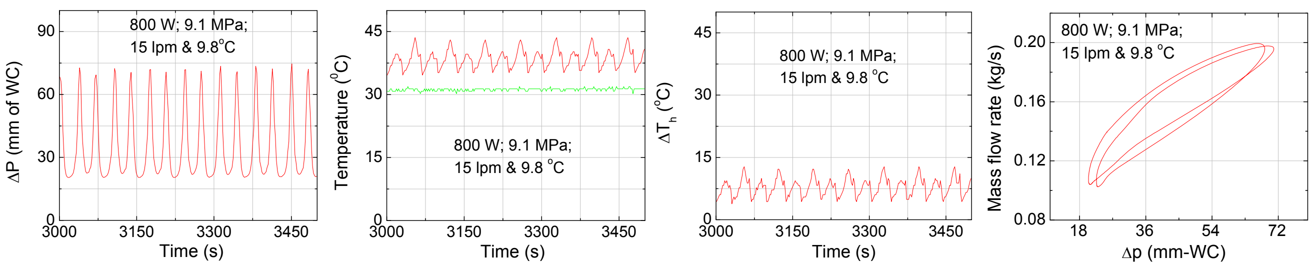

(a) Δp **(b) T_{hi} and T_{ho}** **(c) ΔT_h** **(d) Phase plot**

Fig. 23: Time series and phase plot for the instability shown in Fig. 15b

5.1 With Open-loop Boundary Conditions

In an open-loop, the heater inlet fluid temperature is fixed irrespective of the heater power. For this analysis, all the heat supplied to the heater is assumed to be rejected in the cooler. Further, the operating pressure of the loop, inlet fluid temperature to the heater and the heater power are specified along with the entire geometry of the loop (hydraulic diameter, flow area and length of each pipe section).

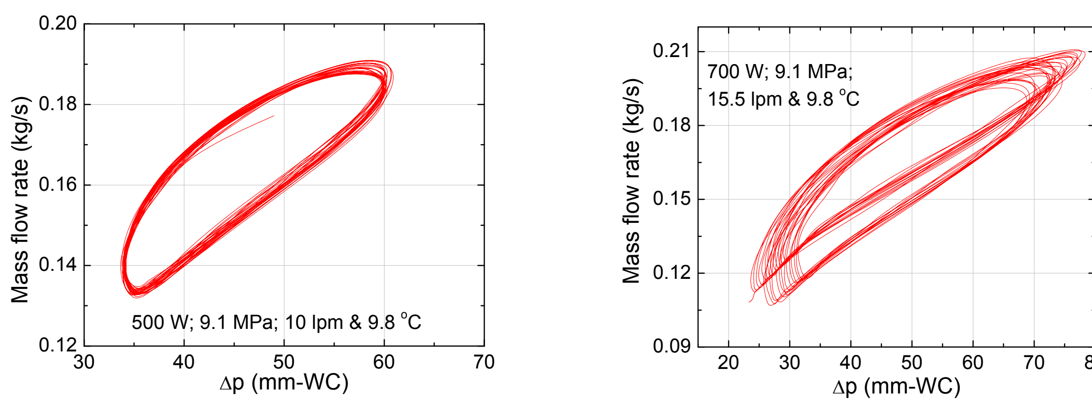

(a) 500 W **(b) 700 W**

Fig. 24: Long duration phase plots

NOLSTA code has been validated for open loop analysis with experimental data available in literature. Lomperski et al. [18] have reported experimental natural circulation data for carbon-dioxide at supercritical pressure for constant heater inlet temperature irrespective of power. The loop orientation is HHHC having ID of 13.88 mm and height of 2 m. The code predicts the steady state mass flow rate and heater outlet temperature appreciably well as shown in Fig. 25.

The code predicts the threshold of instability as 9.8 kW (see Fig. 26) for this loop, whereas no instability has been observed during the experiments.

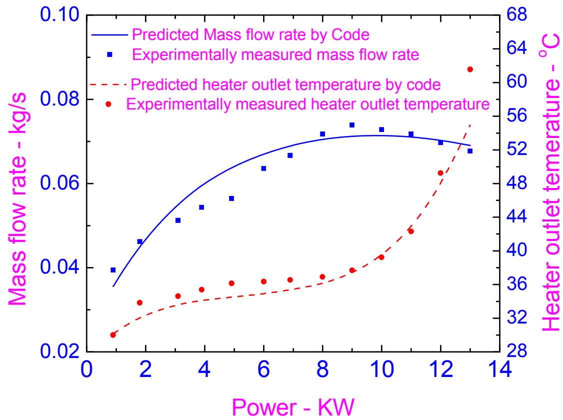

Fig. 25: Measured and predicted data of Lomperski et al. [18] at 8 MPa and 24 °C heater inlet temperature

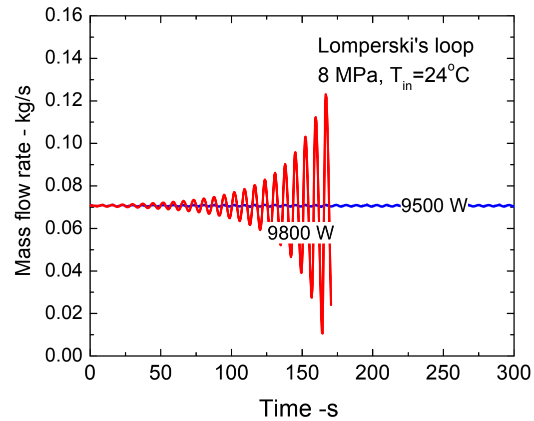

Fig. 26: Instability prediction for Lomperski et al. [18] loop

A parametric analysis has been carried out to study the effect of pressure and heater inlet temperature on the steady state behaviour of SPNCL (HHHC orientation and considering it as an open loop) with carbon-dioxide at supercritical pressures. The mass flow rate increases with pressure at high powers in the friction dominant regime just as in two-phase NC systems as shown in Fig. 27. The steady state natural circulation mass flow rate reduces significantly when heater inlet temperature exceeds the pseudo-critical temperature (e.g. 37^{o}C to 43^{o}C) as shown in Fig. 28. This is attributed to the reduction in the density difference between hot leg and cold-leg resulting in reduced buoyancy head and increase in the frictional resistance as both the legs become supercritical.

Considering the nature of the instability with no perturbation coming at heater inlet temperature, SPNCL stability map was generated for HHHC orientation considering it as an open loop. The stability map so generated is given in Fig. 29 which shows that the loop should have been completely stable for all the operating powers for HHHC orientation as the maximum power was limited to 2.4 kW during the present experiments. The stability threshold for open loop boundary conditions has been found to be very less sensitive to the number of control volumes used for analysis. Hence 28 control volumes have been used for generating the stability map (Sharma et al. [24]). A typical stable and unstable case considering constant heater inlet temperature for HHHC orientation at 9.1 MPa is shown in Fig. 30a. Figure 30b shows the temperature oscillations for the unstable case which indicates the ever increasing amplitude of temperature oscillation at heater outlet leading to flow reversal, whereas heater inlet temperature remains constant. NOLSTA code at present cannot handle flow reversal. However, the heater outlet temperature oscillations observed during experiment achieve a limit cycle without any flow reversal (see figures 21 to 23).

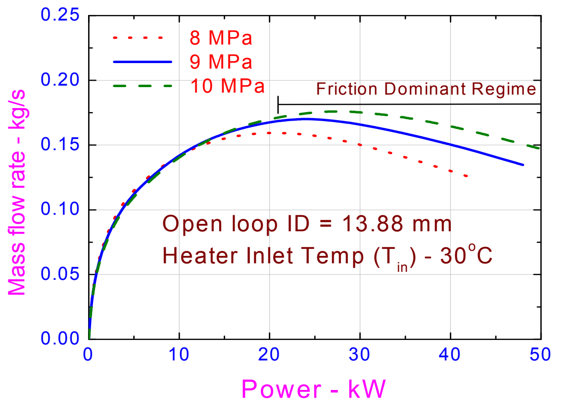

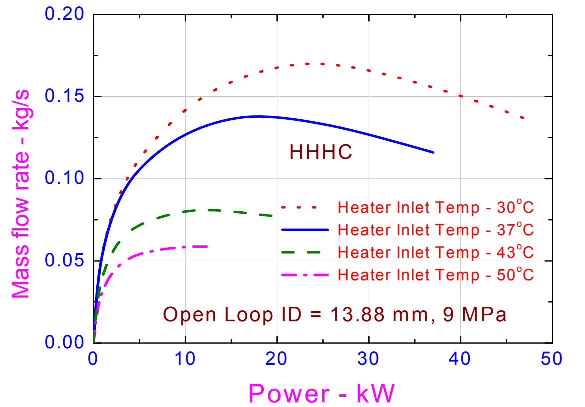

Fig. 27: Effect of pressure on steady state mass flow rate for HHHC orientation

Fig. 28: Effect of heater inlet temperature on steady state mass flow rate for HHHC orientation.

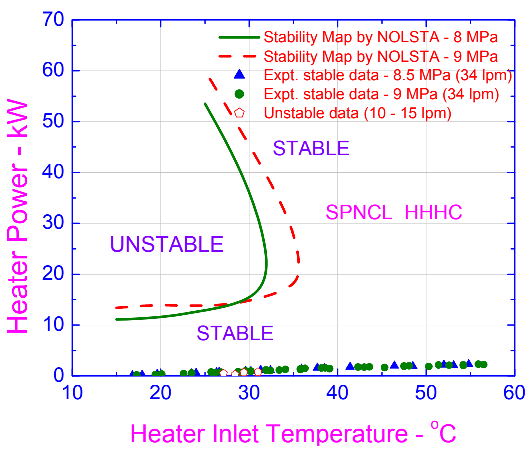

Fig. 29: Comparison of experimental data with stability maps generated by NOLSTA code considering SPNCL as open loop for HHHC orientation

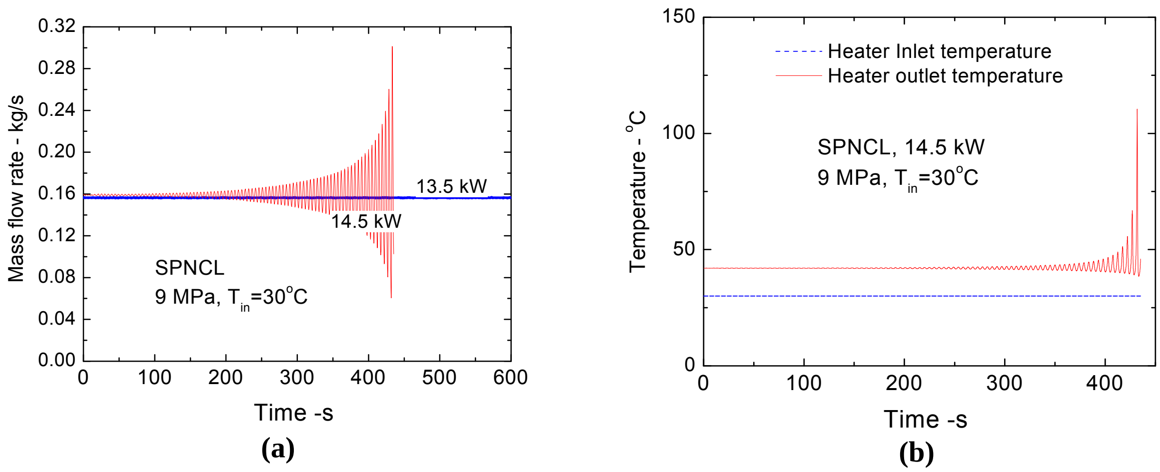

Fig. 30: Typical unstable behaviour at 14.5 kW for open loop SPNCL with HHHC orientation

5.2 With Closed-loop Boundary Conditions

In a closed loop the coolant mass flow rate on secondary side of cooler (i.e. chilled water in SPNCL) and its inlet temperature is kept constant as heater power is increased. The heater inlet temperature is not fixed and increases with increase in heater power. For analysis of closed loop, the rate of heat rejection in the cooler is evaluated based on the calculated overall heat transfer coefficient for cooler and temperature difference between the primary and secondary fluid. In this case, the operating pressure of the loop, coolant mass flow rate & inlet temperature for secondary side of cooler and the heater power are specified along with the entire geometry of the loop (hydraulic diameter, flow area and length of each pipe section).

The stability analysis was carried out for HHHC orientation considering closed loop boundary conditions in which the heater inlet temperature is not specified. The results of the analysis are shown in Fig. 31a & b. The loop is found to be stable at 600 W, becomes unstable at 800 W, continues to be unstable at 1400 W and again becomes stable at 2100 W as shown in Fig. 31a. The instability is predicted for heater inlet temperature varying from 29 to 63 ^{o}C (spread across pseudo-critical temperature of 40^{o}C at 9.1 MPa) as shown in Fig. 31b. Thus, the code is predicting larger unstable zone as compared to the experiment. The stability threshold for closed loop boundary conditions has been found to be sensitive to the number of control volumes used for analysis (i.e. 28 control volumes predict instability from 900 W – 1800 W). Hundred control volumes have been used in the present analysis with closed loop boundary conditions.

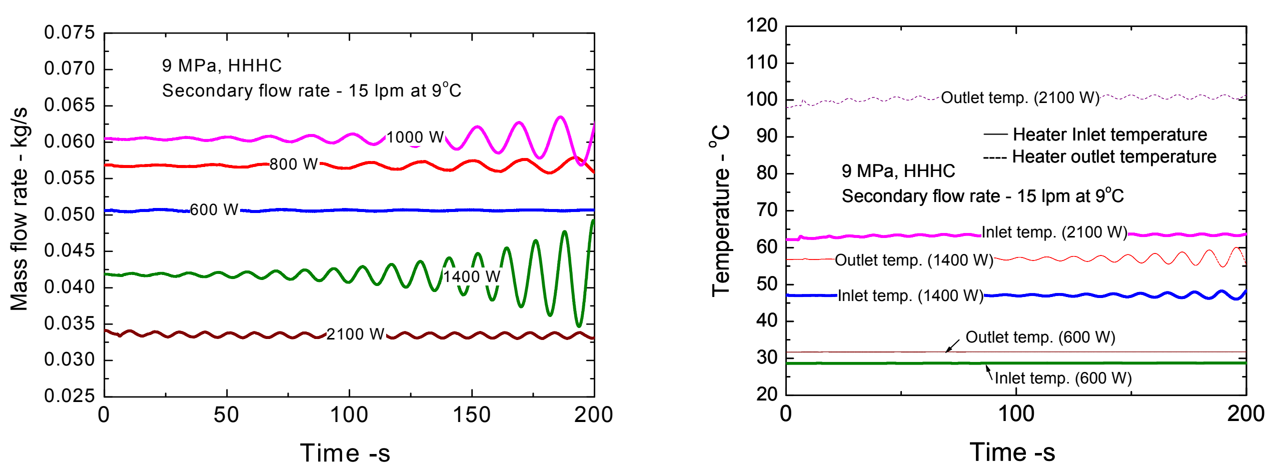

(b) Flow rate variation (b) Temperature variation

Fig. 31: Stability predictions for closed loop SPNCL with HHHC orientation

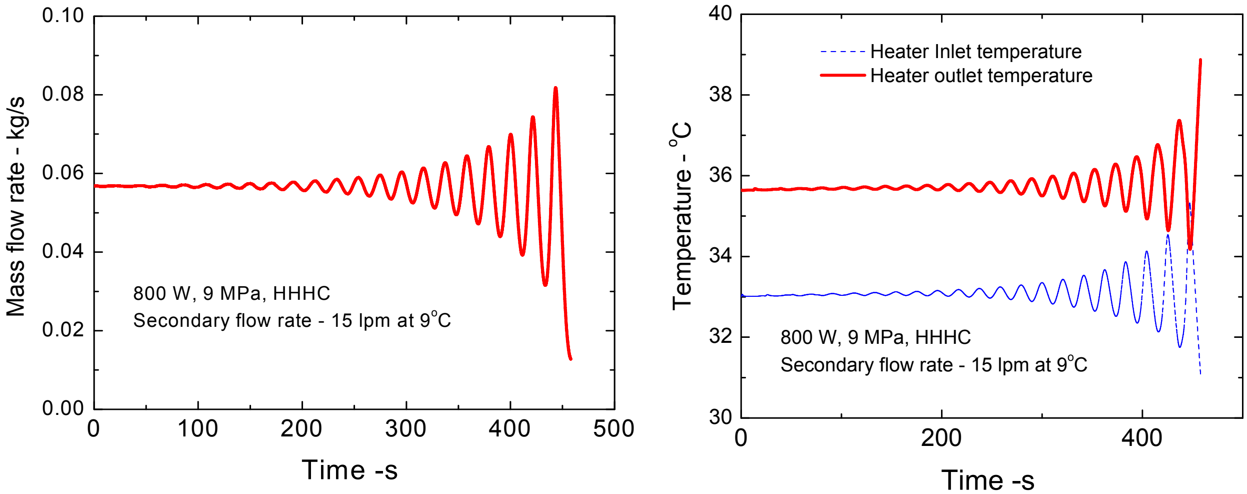

(a) **(b)**

Fig. 32: Prediction of instability at 800 W by NOLSTA code in more detail

Typical unstable behaviour predicted by NOLSTA code at 800 W is shown in more detail in Fig. 32a & b. Fig. 32a shows continuously increasing amplitude of flow oscillations up to flow reversal. Fig. 32b shows increasing amplitude of both heater inlet and outlet temperature oscillations having time period of 22.3 s (steady state loop circulation time of 25.5 s) indicating oscillation growth as the mechanism for development of instability as predicted by Welander for single-phase flow [32]. The Welander mechanism is observed for instability development from steady state condition for SPNCL also as shown in figures 14-16. This is typical for development of instability during sub-critical single phase natural circulation which mostly leads to flow reversal, whereas, no flow reversal was observed during the experiments.

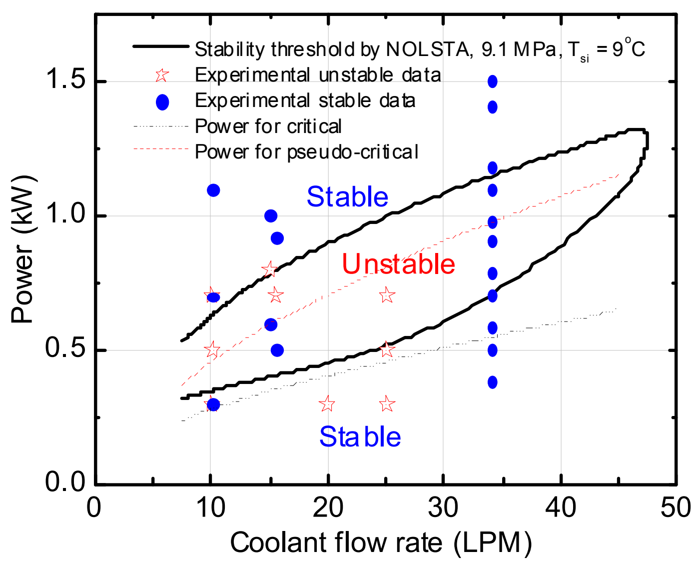

Fig. 33: Prediction of stability map

Fig. 33 shows the predicted stability map for the loop as a function of the secondary mass flow rate. The predictions are made for a pressure of 9.1 MPa. The stable and unstable test data are also shown in this figure. As expected the code predicts a larger unstable zone presumably due to neglect of heat losses, boundary wall effect, axial heat conduction and multidimensional effects.

6.0 CONCLUDING REMARKS

A research program on the supercritical pressure natural circulation is ongoing at BARC as part of the Research Contract 14344 for the IAEA CRP on 'Heat Transfer Behaviour and Thermo-Hydraulics Code Testing for SCWRs'. As part of this, supercritical pressure natural circulation experiments are proposed to be carried out with CO_2 as well as water. Currently, steady state and stability experiments were completed with supercritical CO_2. The steady state flow rate data obtained were compared with the predictions of 1-D code NOLSTA which showed good agreement. Instability was observed in the loop in a narrow window around the pseudo critical region with low cooling water flow rate for the HHHC orientation. All other orientations of heater and cooler were found to be stable. The stability data were compared with the predictions of nonlinear stability analysis code. The analysis was also done with the open-loop and the closed-loop boundary conditions. The analysis with the open-loop boundary conditions did not show instability whereas closed-loop boundary conditions could predict instability. The heat transfer coefficient was measured for subcritical water and supercritical CO_2. The supercritical heat transfer coefficient data showed a peak around the pseudocritical point. The measured heat transfer coefficient data was compared with different correlations reported in the literature. Good agreement was obtained with the McAdams [30] Jackson [31] and Jackson-Fewster [28] correlations.

NOMENCLATURE

A	Flow area (m^2)
b	Constant
C_p	Specific heat (J/kg/k)
D	Hydraulic diameter (m)
f	Friction factor
g	Acceleration due to gravity (m/s^2)
Gr_m	Modified Grashoff Number
i	Enthalpy (j/kg/k)
k	Thermal conductivity (W/m/k)
K	Local Loss coefficient
L	Length (m)
Nu	Nusselt number
p	Constant
ΔP	Pressure drop (Pa)

q	Heat flux (W/m^2)
Q	Heater Power (W)
r_o	Outside radius (m)
r_i	Inside radius (m)
Re	Reynolds number
T	Temperature (^oC)
w	Mass flow rate (kg/s)
Δz	Elevation difference between centre of heater and centre of cooler (m)

Greek

ρ	Density (kg/m^3)
β	Volumetric expansion coefficient (k^{-1})
μ	Dynamic viscosity (Pa-s)

Subscripts

b	bulk
c	cooler
ci	Cooler inlet
co	Cooler outlet
h	heater
ho	Heater outlet
hi	Heater inlet
m	Measured
pc	Pseudocritical
wo	Heater outer wall
wi	Heater inner wall

REFERENCES

1) M.J. Driscoll & P. Hejzlar, 300 MWe Supercritical CO2 Plant Layout and Design, Report No: MIT-GFR-014, MIT Nuclear Engineering Department, June 2004.
2) S.K.S. Tom and E.G. Hauptmann, The feasibility of cooling heavy water reactors with supercritical fluids, Nuclear Engineering and Design 53 (1979) 187-196.
3) J. Buongiorno and P.E. MacDonald, Supercritical water reactor (SCWR) - Progress report for the FY-03 Generation-IV R&D activities for the development of the SCWR in the U.S., INEEL-EXT-03-01210, September 2003.
4) Y. Oka and S. Koshizuka, Supercritical pressure, once-through cycle light water cooled reactor concept, Journal of Nuclear Science & Technology, 38 (2001) 1081-89.

5) R.B. Duffey and K. Hedges, Future CANDU reactor development, ICONE-7459, ICONE-7, Tokyo, April 19-23, Tokyo, Japan, 1999.
6) J. Starflinger, N. Aksan, D. Bittermann, L. Heikinheimo, C. Maraczy, G. Rimpault, T. Schulenberg, Roadmap for Supercritical-Water-Cooled Reactor R&D in Europe, ICAPP'03 May 4-7, 2003, Cordoba, Spain
7) V. Chatoorgoon, A. Voodi and D. Fraser, The stability boundary for supercritical flow in natural-convection loops Part I: H2O studies, Nuclear Engineering and Design 235 (2005) 2570–2580.
8) T.O. Gomez, A. Class, R.T. Lahey Jr., and T. Schulenberg, Stability analysis of a uniformly heated channel with supercritical water, Nuclear Engineering and Design 239 (2009) 2952–2963.
9) V. Chatoorgoon, A. Voodi and P. Upadhyay, The stability boundary for supercritical flow in natural-convection loops Part II: CO2 and H2, Nuclear Engineering and Design 235 (2005) 2581–2593.
10) P.K. Jain, Rizwan-uddin, Numerical analysis of supercritical flow instabilities in a natural circulation loop, Nuclear Engineering and Design 238 (2008) 1947-1957.
11) L. Chen, Xin-Rong Zhang, H. Yamaguchi, Zhong-Sheng (Simon) Liu, Effect of heat transfer on instabilities and transitions of supercritical CO2 flow in a natural circulation loop, International Journal of Heat and Mass Transfer 53 (2010) 4101-4111.
12) C.P. Marcel, M. Rhode, V.P. Masson and T.H.J.J. Van der Hagen, Fluid-to-fluid modeling of supercritical water loops for stability analysis, International Journal of Heat and Mass Transfer 52 (2009) 5046-5054.
13) Walter Ambrosini, Discussion on the stability of heated channels with different fluids at supercritical pressures, Nuclear Engineering and Design 239 (2009) 2952–2963.
14) W. Ambrosini, M. Sharabi, Dimensionless parameters in stability analysis of heated channels with fluids at supercritical pressures, Nuclear Engineering and Design, 238(2008) 1917-1929.
15) Xin-Rong Zhang, L. Chen, H. Yamaguchi, Natural convective flow and heat transfer of supercritical CO2 in a natural circulation loop, International Journal of Heat and Mass Transfer 53 (2010) 4112-4122.
16) V.A. Silin, V.A. Voznesensky and A.M. Afrov, The light water integral reactor with natural circulation of the coolant at supercritical pressure BF-500 SKDI, Nuclear Engineering and Design 144 (1993) 327-336.
17) Bushby, S.J., Dimmick, G.R., Duffey, R.B., Spinks, N.J., Burrill, K.A. and Chan, P.S.W., Conceptual designs for advanced, high-temperature CANDU reactors, SCR-2000, Nov.6-8, 2000, Tokyo.
18) Lomperski, S., Cho, D., Jain, R., Corradini, M.L., 2004. Stability of a natural circulation loop with a fluid heated through the thermodynamic pseudocritical point. In: Proceedings of ICAPP '04, Pittsburgh, PA, USA, June 13–17, Paper 4268.
19) Holman J.P and Boggs, J.H., Heat transfer to freon 12 near the critical state in a natural circulation loop, J. Heat Transfer 82 (1960) 221-226.

20) Yoshikawa, S., R.L. Smith Jr., H. Inomata, Y. Matsumura and K. Arai, Performance of a natural convection circulation system for supercritical fluids, J. of Supercritical Fluids 36 (2005) 70-80.
21) Shiralkar, B.S., Griffith, P., Deterioration in heat transfer to fluids at supercritical pressures and high heat fluxes. J. Heat Transfer, Trans. ASME 91 (1), 27–36, 1969.
22) Pioro, I.L. and R. B. Duffey, Heat transfer and hydraulic resistance at supercritical pressures in power engineering applications, ASME press, Three Park Avenue, New York, NY 10016, USA.
23) Swapnalee, B.T. and Vijayan P.K., A generalized flow correlation for single-phase natural circulation loops obeying multiple friction laws, Communicated to International Journal of Heat and Mass Transfer.
24) M. Sharma, P.K. Vijayan, D.S. Pilkhwal, D. Saha and R.K. Sinha, Linear and non-linear stability analysis of a supercritical natural circulation loop, ASME Journal of Engineering for Gas Turbines and Power, October 2010, Vol. 132 / 102904-1.
25) Bringer, R.P., Smith, J.M., Heat transfer in the critical region, AIChE J. 3 (1), 49–55, 1957.
26) Bishop, A.A., Sandberg, R.O., Tong, L.S., Forced convection heat transfer to water at near-critical temperatures and supercritical pressures, Report WCAP-2056, Part IV, November, Westinghouse Electric Corp., Pittsburgh, USA, 1964.
27) Yamagata, K., Nishikawa, K., Hasegawa, S., Forced convective heat transfer to supercritical water flowing in tubes, Int. J. Heat Mass Transfer 15 (12), 2575–2593, 1972.
28) Jackson, J.D., Fewster, J., Forced convection data for supercritical pressure fluids, HTFS 21540, 1975.
29) Shitsman, M.E., Heat transfer to water, oxygen and carbon-dioxide in near critical region (In Russian), Thermal Eng. 1, 68–72, 1959.
30) McAdams, W.H., Heat Transmission, 2nd edition, McGraw-Hill, New York, NY, USA, 1942.
31) Jackson, J.D., Consideration of the heat transfer properties of supercritical pressure water in connection with the cooling of advanced nuclear reactors. In: Proceedings of the 13th Pacific Basin Nuclear Conference, Shenzhen City, China, October 21–25, 2002.
32) Welander, P., On the oscillatory instability of a differentially heated loop, J. Fluid Mech. (1967) 29 17-30.
33) P.K. Vijayan, A.K. Nayak, D. Saha and M.R.Gartia, Effect of loop diameter on the steady state and stability behaviour of single-phase and two-phase natural circulation loops, Science and Technology of Nuclear Installations, Vol. 2008, Article ID 672704.
34) B.M. Lingade, Heat transfer and stability studies on supercritical natural circulation loop, M.Tech. thesis, 2010, Homi Bhabha National Institute, Mumbai 400094, India.

Appendix-1: Steady state natural circulation data with CO_2

Steady state natural circulation data generated with CO_2 are given in tables A1-1, A1-2, A1-3 and A1-4 are generated respectively for the HHHC, HHVC, VHHC and VHVC orientations. For the HHHC orientation data are available for the clockwise and counterclockwise directions.

Table A1-1: Steady state data for HHHC orientation (clockwise flow)

Sr. No.	Power (W)	PTr-1 (bar)	T1 (°C)	T2 (°C)	T3 (°C)	T4 (°C)	T5 (°C)	T6 (°C)	T7 (°C)	T8 (°C)	T9 (°C)	T10 (°C)	T11 (°C)	T12 (°C)	T13 (°C)	T14 (°C)	T15 (°C)	T16 (°C)	T17 (°C)	T18 (°C)	T-33 (°C)	T-34 (°C)	T-35 (°C)	T-36 (°C)	T-37 (°C)	T-38 (°C)	T-41 (°C)	T-42 (°C)	LPM$	Mass* flow rate
1	203.7	84.7	17.4	17.9	22.5	23.3	23.7	faulty	24.7	23.3	24.7	23.9	25.5	24.1	25.2	23.5	20.3	20.1	20.2	20.2	21.4	21.5	17.3	18.1	17.5	17.2	9.2	10.0	37.0	0.02818
2	387.9	84.7	19.0	19.6	27.0	28.9	28.6	faulty	30.3	28.3	31.5	29.5	31.6	28.6	31.4	28.6	23.2	22.4	22.5	23.0	24.2	24.1	19.6	20.3	19.7	19.9	8.8	9.7	37.0	0.03841
3	590.5	85.0	23.0	23.5	32.6	35.0	34.7	faulty	35.9	33.3	37.1	34.5	37.1	33.7	37.5	33.6	26.5	26.8	27.0	27.5	27.6	27.9	23.5	24.3	23.5	23.2	9.0	9.8	37.0	0.04393
4	785.3	85.3	26.3	26.8	37.1	39.4	39.1	faulty	40.9	37.2	42.2	39.5	41.6	38.2	42.0	38.7	29.9	30.2	30.4	30.3	30.9	30.6	26.3	28.2	27.0	27.0	8.7	9.7	37.0	0.05388
5	977.5	85.3	29.1	29.6	39.9	42.7	42.4	faulty	44.3	40.0	45.5	42.3	44.9	40.4	44.8	40.9	32.8	32.4	32.6	33.7	34.3	34.2	29.1	31.6	30.1	30.1	8.8	9.5	37.0	0.05367
6	1184.0	84.7	31.4	31.3	41.0	43.8	43.0	faulty	45.4	41.7	46.7	43.4	45.4	41.5	46.5	42.0	33.9	34.1	34.3	34.8	34.9	34.9	30.8	32.8	31.6	31.4	8.9	9.7	37.0	0.05635
7	1406.2	85.6	35.8	35.8	44.9	51.0	47.4	faulty	48.8	46.1	49.5	46.2	49.3	45.5	49.3	45.4	37.8	36.9	37.7	37.6	38.2	38.4	35.8	37.3	36.4	36.6	9.0	9.9	35.5	0.05144
8	1103.0	86.3	31.9	32.4	41.0	44.9	43.5	faulty	44.9	41.7	46.1	42.9	45.4	42.1	45.9	42.0	35.0	34.6	34.9	35.9	35.4	35.6	32.5	33.9	32.8	32.7	8.9	9.7	35.5	0.05183
9	702.9	84.7	26.3	26.3	34.3	37.7	36.3	faulty	37.6	35.6	38.8	36.7	38.2	35.4	38.7	35.9	29.4	29.1	29.8	29.7	30.4	30.2	26.9	27.1	26.9	27.1	9.3	10.0	34.80	0.05284
10	1593.7	85.1	37.0	37.5	48.9	56.0	53.4	faulty	55.5	49.4	59.0	52.3	56.5	50.5	58.3	51.0	39.0	39.1	39.4	39.8	40.5	40.6	37.5	39.0	38.0	37.8	9.0	10.0	36.00	0.04476
11	1798.0	85.8	40.9	41.4	65.7	77.7	75.4	faulty	84.7	73.3	91.1	77.4	90.3	75.8	94.1	78.4	49.1	49.2	51.2	51.6	51.7	51.4	40.8	42.3	41.9	41.7	9.0	10.0	34.80	0.03944
12	2000.5	84.7	45.9	46.4	89.3	103.7	102.4	faulty	117.2	103.3	125.9	109.7	126.3	108.4	132.2	112.6	63.2	65.9	69.2	69.6	69.2	69.0	44.8	46.9	46.1	45.7	9.1	10.1	33.50	0.03599
13	2197.7	85.0	50.9	52.0	114.6	132.0	130.5	faulty	150.3	133.3	159.7	142.0	160.7	140.9	168.1	146.8	80.7	84.4	88.9	89.8	87.1	87.2	49.8	51.9	51.8	51.4	9.0	11.0	34.70	0.03104
14	2287.0	85.3	54.9	54.8	126.4	145.4	143.2	faulty	164.8	148.3	175.4	156.4	175.6	155.5	183.8	161.9	89.2	93.3	98.5	98.8	96.1	96.3	52.6	54.8	55.4	55.8	9.2	10.4	33.00	0.03028
15	2077.1	85.0	52.6	53.1	114.0	130.9	128.3	faulty	149.7	133.9	159.1	142.0	159.6	140.4	166.4	146.8	82.4	85.5	90.6	90.9	89.4	89.7	50.9	52.5	53.5	53.0	9.5	11.2	35.40	0.03009
16	1916.1	85.0	48.2	48.6	96.1	111.0	109.6	faulty	126.1	112.2	134.4	118.6	134.6	116.8	140.6	122.1	69.4	72.1	75.4	75.8	75.3	75.2	47.0	49.1	49.1	48.9	9.5	10.9	34.20	0.03265
17	1497.7	84.4	38.6	38.6	52.8	60.5	59.5	faulty	64.5	56.7	68.0	59.0	68.1	58.4	70.6	59.4	41.2	41.3	42.8	43.2	43.3	43.5	38.6	39.5	39.0	39.1	9.3	10.6	33.70	0.04299
18	198.6	89.8	17.4	18.4	22.5	23.9	23.7	faulty	24.7	23.9	25.3	24.5	25.5	24.5	25.2	24.6	20.3	20.1	20.8	21.3	21.4	19.5	17.3	18.6	18.6	19.6	9.5	10.2	30.0	0.02259
19	398.0	90.2	21.8	22.4	29.2	31.6	31.4	faulty	33.1	30.6	33.7	31.7	34.3	31.4	34.2	31.9	25.4	24.6	25.9	26.9	26.4	24.5	21.3	23.1	23.1	24.8	9.3	10.2	30.1	0.03024
20	597.3	90.0	24.6	25.2	34.8	37.7	37.4	faulty	38.7	36.1	39.9	37.3	40.4	37.6	39.8	37.0	28.8	28.5	30.4	30.9	29.8	28.4	25.2	26.0	26.4	28.0	9.4	10.3	30.0	0.02968
21	789.3	90.0	28.0	28.5	39.3	42.2	41.3	faulty	43.2	40.0	44.4	41.2	44.3	41.0	44.3	40.3	31.6	31.8	33.2	34.2	32.6	31.2	28.0	29.4	29.3	30.7	9.4	10.3	30.0	0.03576
22	1003.7	90.2	31.4	31.9	42.7	46.6	45.7	faulty	47.1	43.9	48.3	45.7	48.2	44.4	48.2	44.3	35.0	35.2	36.0	37.1	36.5	34.5	31.9	33.3	33.2	35.2	9.3	10.5	30.0	0.03909
23	1215.6	90.2	34.7	35.8	45.5	48.8	48.5	faulty	49.9	46.7	51.2	47.9	51.5	47.2	51.5	46.5	37.8	37.4	38.3	39.3	38.2	36.7	34.7	36.1	36.0	38.0	9.5	10.5	30.0	0.04441
24	1413.6	90.0	37.5	38.0	47.2	52.1	51.8	faulty	53.3	49.4	55.7	50.7	54.8	50.0	55.5	49.9	39.5	39.7	41.5	40.5	40.5	38.4	37.5	39.0	38.8	41.4	8.9	9.9	30.0	0.03791
25	1616.0	90.8	40.3	40.8	53.9	61.0	59.5	faulty	63.3	56.7	66.3	58.5	66.5	57.3	67.8	57.7	42.9	43.0	44.5	45.5	44.4	42.8	40.8	42.3	41.6	44.2	9.3	10.5	30.0	0.03885
26	1800.0	90.4	44.2	44.2	68.0	78.2	76.5	faulty	85.2	74.4	90.0	77.9	89.2	76.9	92.4	77.9	50.8	52.0	54.0	55.6	54.0	51.2	43.6	45.2	45.6	47.5	9.5	10.5	30.2	0.04034
27	2399.1	90.2	57.7	58.1	128.7	146.5	144.3	faulty	167.6	150.0	177.7	157.6	177.3	157.2	184.9	162.5	90.9	95.0	100.2	101.6	97.3	95.7	55.4	58.2	59.6	62.1	10.2	11.7	30.0	0.03136
28	2305.5	90.3	52.1	52.6	124.7	143.1	140.9	faulty	162.6	146.7	172.6	153.7	172.3	153.3	179.3	158.0	89.8	93.3	98.5	99.9	96.7	95.1	54.8	57.6	60.2	62.1	9.7	11.7	30.0	0.03109
29	1905.0	89.8	47.6	48.1	83.1	96.5	94.7	faulty	107.6	65.0	114.7	100.2	114.1	99.4	119.3	102.0	61.0	62.6	66.4	67.4	66.3	64.0	46.4	48.0	49.5	51.4	8.9	10.1	29.8	0.03653
30	1717.3	89.1	43.1	43.6	65.7	76.0	74.3	faulty	81.9	71.7	87.1	75.2	87.5	75.2	90.8	76.8	49.7	50.3	52.9	53.9	52.8	50.6	43.1	44.6	45.1	47.0	8.8	10.4	29.8	0.03944
31	1500.2	87.9	39.7	40.3	51.1	58.3	56.2	faulty	60.5	54.4	63.0	56.2	63.2	55.0	65.0	56.0	41.8	41.3	43.8	42.8	43.3	41.2	39.7	40.6	40.1	43.1	8.8	10.4	29.8	0.05081
32	907.8	89.1	31.9	32.4	41.6	46.0	44.0	faulty	46.0	42.8	46.7	43.4	46.5	43.2	46.5	43.1	35.0	35.2	36.0	36.5	36.0	34.5	31.3	33.3	33.2	35.2	9.4	10.6	29.6	0.03757
33	703.1	89.6	28.0	28.5	37.6	41.6	39.6	faulty	41.5	39.4	42.7	40.1	42.1	39.9	42.0	39.2	31.6	31.3	33.7	32.7	32.6	31.2	29.0	29.4	29.8	31.3	9.3	10.3	29.8	0.0353
34	491.1	89.1	23.5	24.6	31.5	34.4	33.6	faulty	34.8	33.3	36.0	34.0	36.0	33.7	36.4	33.6	27.1	26.8	28.1	28.6	28.1	26.7	23.5	24.8	25.3	26.3	9.3	10.3	29.8	0.03454
35	302.0	89.8	20.7	20.7	26.4	28.3	28.1	faulty	29.2	27.8	30.4	28.9	30.5	28.6	30.3	29.1	23.7	23.5	25.3	24.2	24.7	22.8	20.1	21.5	21.9	22.9	9.4	10.2	29.8	0.02497

Table A1-1: Steady state data for HHHC orientation (anti-clockwise flow)

Sr. No.	Power (W)	PTr-1 (bar)	T1 (°C)	T2 (°C)	T3 (°C)	T4 (°C)	T5 (°C)	T6 (°C)	T7 (°C)	T8 (°C)	T9 (°C)	T10 (°C)	T11 (°C)	T12 (°C)	T13 (°C)	T14 (°C)	T15 (°C)	T16 (°C)	T17 (°C)	T18 (°C)	T-33 (°C)	T-34 (°C)	T-35 (°C)	T-36 (°C)	T-37 (°C)	T-38 (°C)	T-41 (°C)	T-42 (°C)	LPM$	Mass* flow rate
1	100.1	85.4	19.0	19.6	21.3	22.7	22.6	Faulty	22.4	22.8	22.5	21.7	22.2	28.8	21.3	20.7	18.6	17.9	18.6	19.1	18.0	16.7	20.1	22.0	20.3	20.9	10.8	11.4	10.0	0.02280
2	246.8	85.2	23.5	23.5	28.1	29.4	29.7	Faulty	29.7	28.3	29.2	28.4	28.8	26.9	28.0	27.5	22.0	21.8	22.0	23.6	21.4	20.6	25.2	26.0	25.4	25.9	10.9	11.7	10.1	0.03870
3	301.0	85.0	25.2	25.2	30.3	33.3	31.9	Faulty	32.0	30.0	31.5	30.6	31.0	29.2	29.7	29.1	23.7	22.9	23.6	24.7	23.0	21.7	26.9	28.2	27.2	27.6	10.8	12.0	10.1	0.04450
4	349.6	85.0	26.3	26.3	31.5	34.4	33.6	Faulty	33.6	31.7	33.2	31.7	32.1	30.3	31.4	30.8	24.8	24.0	24.8	25.8	24.2	23.4	27.4	28.8	27.8	28.2	10.7	12.0	10.1	0.04950
5	399.5	84.8	27.4	27.4	33.1	36.1	35.2	Faulty	35.3	33.3	34.3	33.4	33.8	32.0	33.1	31.9	25.4	25.1	25.3	26.4	24.2	33.9	28.0	29.9	28.6	29.1	10.7	11.6	10.1	0.04340
6	450.9	85.0	28.6	28.5	34.3	37.7	36.3	Faulty	37.0	33.9	36.0	34.5	34.3	33.7	34.2	33.6	26.0	25.7	26.5	27.5	25.9	24.5	29.7	31.1	29.9	30.3	10.5	11.9	10.1	0.03960
7	551.5	84.8	30.2	30.7	37.1	40.5	39.1	Faulty	39.8	37.2	39.4	37.3	38.8	35.9	38.1	36.4	28.8	27.9	30.3	28.7	28.1	27.3	31.9	32.7	32.3	32.4	10.4	11.6	10.1	0.05060
8	601.4	84.8	31.4	31.3	38.3	41.6	40.2	Faulty	40.9	38.3	40.5	38.4	39.3	37.6	38.7	37.5	29.4	29.1	29.8	31.4	28.7	27.8	32.4	34.4	32.9	33.1	10.4	11.6	10.1	0.05270
9	675.8	84.7	33.0	33.5	39.3	42.7	41.3	Faulty	42.0	40.0	42.2	40.1	41.0	38.7	40.3	39.2	31.1	31.3	31.5	32.6	30.9	30.0	34.1	35.6	34.9	34.7	10.3	12.2	10.10	0.03670
10	225.4	85.0	23.5	23.5	27.5	28.8	28.6	Faulty	28.6	27.8	28.7	27.3	28.3	26.4	27.5	26.9	21.8	22.0	23.6	22.0	21.4	20.6	24.6	26.0	24.7	25.2	10.8	11.7	10.00	0.03220
11	274.5	85.3	24.6	25.2	29.2	31.6	31.4	Faulty	31.4	29.4	30.9	29.5	29.9	29.2	29.7	28.6	23.1	22.9	23.6	24.7	22.5	21.7	26.3	27.7	26.0	26.5	10.9	11.9	10.10	0.03180
12	324.6	86.1	26.3	26.8	30.9	34.4	32.5	Faulty	33.6	31.1	33.2	31.7	32.1	33.9	31.4	30.3	24.3	24.0	24.8	25.8	23.6	22.8	27.4	29.4	28.0	27.9	10.8	11.9	10.00	0.03130
13	375.7	85.0	27.4	28.0	32.6	36.6	34.7	Faulty	34.8	33.3	34.3	33.4	33.8	32.6	33.1	31.9	26.0	25.1	25.9	26.9	25.3	24.5	29.1	30.5	29.4	29.7	10.6	11.7	10.00	0.04000
14	427.0	84.6	29.1	29.1	34.3	37.7	36.9	Faulty	37.0	35.0	36.5	35.1	35.5	34.2	34.7	33.6	27.1	26.8	28.6	27.0	26.4	25.6	30.2	31.6	30.9	30.7	11.0	12.4	10.00	0.04230
15	473.2	84.6	30.2	30.7	36.0	38.8	38.0	Faulty	38.7	36.1	38.2	36.1	37.1	35.4	36.4	35.9	28.8	27.9	28.7	29.8	27.5	26.7	31.3	32.7	32.1	31.9	11.1	12.4	10.00	0.04300
16	528.7	84.8	31.4	31.3	37.1	39.9	39.1	Faulty	39.8	37.8	39.4	37.9	38.8	37.1	38.1	37.0	29.1	29.4	30.9	29.8	28.7	27.3	32.4	33.9	32.2	33.0	11.2	12.8	10.20	0.04180
17	574.0	84.7	31.9	32.4	37.6	40.5	39.6	Faulty	40.4	38.9	40.5	39.0	39.3	38.2	39.2	38.7	29.6	30.5	31.0	32.0	29.8	28.9	33.6	35.0	33.8	33.5	11.2	12.8	10.10	0.03560
18	626.0	84.7	33.0	33.5	38.2	42.2	40.7	Faulty	41.5	38.9	41.0	39.5	40.4	38.7	39.8	39.2	31.1	31.3	31.5	32.6	30.4	30.0	33.6	35.6	34.9	34.7	11.3	12.9	10.1	0.0339
19	680.1	85.0	34.1	34.1	39.9	42.7	41.3	Faulty	42.0	40.0	42.2	40.6	41.0	39.3	40.3	39.2	31.8	32.2	32.1	33.7	31.5	30.6	34.7	36.1	35.4	35.8	10.9	12.8	10.0	0.0365
20	772.2	85.6	35.8	35.8	41.6	44.9	42.9	Faulty	44.3	41.7	43.9	42.3	43.8	41.0	43.1	42.0	34.1	34.4	35.5	35.9	33.7	32.8	36.4	38.4	37.1	37.5	11.8	13.3	10.0	0.0334
21	849.5	85.0	35.3	35.8	41.0	44.9	43.5	Faulty	44.3	41.7	44.4	41.8	43.8	41.5	42.6	42.0	33.5	34.4	34.3	35.9	33.2	32.8	36.4	37.8	36.8	37.1	10.3	12.1	10.2	0.0296

Table A1-2: Steady state data for HHVC orientation

Sr. No.	Power (W)	PTr-1 (bar)	T1 (°C)	T2 (°C)	T3 (°C)	T4 (°C)	T5 (°C)	T6 (°C)	T7 (°C)	T8 (°C)	T9 (°C)	T10 (°C)	T11 (°C)	T12 (°C)	T13 (°C)	T14 (°C)	T15 (°C)	T16 (°C)	T17 (°C)	T18 (°C)	T33 (°C)	T34 (°C)	T37 (°C)	T38 (°C)	T39 (°C)	T40 (°C)	T43 (°C)	T44 (°C)	LPM	Mass flow rate
1	395.9	85.8	19.6	20.7	30.0	28.7	30.3	faulty	32.5	29.4	33.7	30.6	34.4	30.3	34.2	31.4	23.7	24.0	24.2	24.7	25.3	25.5	25.3	25.2	19.5	20.6	8.9	9.1	34.0	0.03064
2	820.1	85.8	28.0	27.4	43.8	39.3	42.4	faulty	44.3	40.0	45.5	41.8	46.0	40.4	46.5	41.5	31.6	31.8	32.6	32.5	33.2	33.4	33.2	33.4	27.4	27.9	8.2	8.8	34.1	0.03867
3	987.2	86.1	31.2	31.7	46.6	41.6	44.6	faulty	47.1	42.2	49.5	44.0	48.8	42.7	49.3	43.7	34.4	34.6	34.9	35.3	36.0	36.5	36.0	36.2	30.8	31.4	8.8	9.1	34.5	0.04429
4	1216.9	86.5	34.9	35.4	51.0	44.4	49.0	faulty	51.6	45.6	53.4	47.3	53.2	46.0	53.8	46.5	37.3	36.9	37.1	37.6	38.2	38.7	38.3	38.2	34.8	35.4	8.6	9.0	33.5	0.04618
5	1423.5	85.3	36.4	36.9	54.4	46.6	52.3	faulty	56.1	48.3	58.5	50.1	56.0	48.8	55.5	49.3	38.4	38.0	38.8	38.7	38.8	38.6	39.4	39.6	36.9	36.4	9.1	9.5	34.0	0.04165
6	1604.2	85.3	38.6	39.1	67.7	56.7	66.1	faulty	72.9	61.1	77.6	64.0	77.6	64.0	80.7	66.1	42.3	42.5	43.9	44.3	43.9	43.8	44.4	44.8	38.6	39.2	9.6	10.4	34.2	0.04115
7	1780.0	85.3	42.0	42.5	92.1	77.5	91.4	faulty	104.3	88.9	111.9	94.1	113.0	94.9	117.7	99.7	55.3	56.4	59.1	59.5	59.6	59.8	59.6	59.9	42.0	42.5	9.7	10.2	34.7	0.03211
8	1990.9	85.6	44.2	44.7	107.6	92.7	107.9	faulty	125.0	106.1	133.8	113.0	135.2	115.7	142.3	121.0	63.2	65.9	69.8	70.7	70.3	70.2	68.6	68.5	44.8	44.6	9.1	9.7	34.0	0.03023
9	2186.7	85.6	48.7	49.8	136.5	120.2	138.2	faulty	159.8	140.0	171.5	149.2	174.0	152.7	182.1	159.1	83.0	86.0	92.9	93.2	91.1	91.5	87.8	87.9	49.3	49.7	8.9	10.0	33.9	0.02616
10	1705.0	85.3	40.3	40.8	78.8	66.9	78.2	faulty	89.1	74.4	95.6	79.1	94.2	78.0	98.6	81.8	48.0	48.6	50.6	51.1	51.2	51.5	51.2	51.6	40.9	40.7	8.9	9.3	33.8	0.03678
11	1503.4	85.2	37.5	38.0	60.5	51.1	58.4	faulty	63.9	54.4	68.0	56.2	67.0	55.0	68.9	56.6	40.1	39.7	40.5	40.4	41.0	41.0	41.6	41.9	37.5	37.9	9.1	9.7	34.0	0.04528
12	1099.2	85.3	33.6	33.5	47.7	42.7	46.3	faulty	48.8	43.3	50.6	45.1	50.4	43.8	50.4	43.7	36.1	35.2	36.0	36.5	36.5	36.9	37.7	37.7	33.0	33.7	9.0	9.3	33.5	0.04548
13	900.6	84.4	29.7	30.2	44.4	39.9	43.0	faulty	44.9	40.0	46.1	41.8	46.5	41.0	46.5	41.5	33.3	33.5	33.2	33.7	34.3	34.7	34.9	35.4	29.6	29.9	9.0	9.3	33.7	0.04735
14	700.4	84.4	26.9	27.4	39.9	36.5	39.6	faulty	40.9	38.3	42.2	39.0	42.7	38.2	42.6	38.7	30.5	30.7	30.9	30.8	32.0	32.3	32.6	32.3	26.8	26.7	9.1	9.5	34.0	0.04519
15	499.6	84.2	23.5	24.0	35.5	32.6	35.2	faulty	37.0	33.9	37.7	34.5	37.1	33.7	37.5	34.2	27.1	27.4	27.6	27.5	28.7	28.6	29.3	29.6	23.5	23.9	9.3	9.6	34.8	0.03874
16	300.0	84.7	20.2	20.7	28.9	27.5	29.2	faulty	30.3	28.3	31.5	29.0	32.1	29.2	31.9	30.3	23.7	24.0	24.2	24.1	25.3	25.6	25.9	25.7	20.7	20.3	9.2	9.5	34.0	0.02651

Table A1-3: Steady state data for VHHC orientation

Sr. No.	Power (W)	PTr-1 (bar)	T-17 (°C)	T-18 (°C)	T-19 (°C)	T-20 (°C)	T-21 (°C)	T-22 (°C)	T-23 (°C)	T-24 (°C)	T-25 (°C)	T-26 (°C)	T-27 (°C)	T-28 (°C)	T-29 (°C)	T-30 (°C)	T-31 (°C)	T-32 (°C)	T-33 (°C)	T-34 (°C)	T-35 (°C)	T-36 (°C)	T-37 (°C)	T-38 (°C)	T-41 (°C)	T-42 (°C)	LPM	Mass flow rate
1	148.0	89.6	17.5	17.4	21.3	19.3	23.3	20.7	26.4	26.9	27.9	27.8	26.3	25.3	25.8	26.3	13.5	20.1	20.8	18.4	16.2	18.1	17.4	21.2	10.2	10.9	32.2	0.02380
2	353.5	89.4	21.4	21.9	29.8	27.6	32.9	35.8	39.9	39.3	35.2	34.5	39.2	34.9	36.4	36.4	17.8	25.7	25.3	23.9	21.3	22.0	22.5	25.7	10.9	11.6	32.0	0.05170
3	549.6	89.1	24.8	24.7	35.9	33.6	39.7	42.5	45.5	44.3	40.8	40.6	47.7	42.8	43.1	43.2	22.6	29.1	29.2	27.3	24.6	25.4	25.3	29.1	11.0	11.9	31.9	0.04900
4	756.7	90.2	28.7	28.6	41.0	39.1	44.3	48.7	53.9	50.5	45.8	45.6	58.9	47.9	48.7	48.2	27.5	33.6	33.7	31.7	28.5	29.4	29.8	33.0	11.3	12.4	32.1	0.04850
5	953.1	89.1	31.5	32.0	45.5	43.6	49.4	48.7	58.4	55.5	51.4	50.6	65.6	51.2	52.6	50.5	30.2	35.8	36.0	33.9	31.3	32.2	32.6	37.5	11.4	12.3	32.2	0.06481
6	1555.2	90.4	40.0	39.9	59.5	59.0	63.5	64.3	70.7	67.9	65.9	64.0	85.2	63.1	64.9	65.0	36.1	42.5	42.7	40.6	39.7	40.6	41.1	45.3	11.4	12.5	32.1	0.07632
7	1748.6	91.4	42.2	42.1	69.6	68.4	76.6	80.6	86.5	83.6	82.1	79.0	104.3	79.4	82.9	83.5	41.5	47.6	47.2	45.6	41.4	42.9	42.8	47.5	11.1	12.4	34.8	0.05561
8	1972.2	91.6	43.3	43.8	78.0	77.2	87.4	90.6	98.2	94.8	93.9	91.2	120.5	92.9	98.5	98.7	43.6	51.5	51.5	49.0	42.5	43.5	43.9	48.1	9.3	10.7	37.8	0.05311
9	2195.9	91.2	47.9	47.7	103.3	99.2	123.7	129.2	135.9	131.3	133.0	129.6	162.0	134.0	143.3	144.1	59.3	67.7	67.5	65.1	46.4	47.4	48.4	52.6	9.2	10.3	38.0	0.03971
10	2374.3	92.1	49.5	49.4	116.2	111.4	143.0	148.3	156.6	152.0	156.4	153.0	185.0	155.9	166.8	167.6	67.3	76.6	74.8	72.9	48.1	49.7	50.6	54.8	9.1	10.5	38.0	0.03741
11	2244.3	91.9	49.5	49.4	111.7	106.4	135.6	136.5	149.9	146.4	149.2	145.8	176.0	148.0	159.0	159.8	65.7	74.4	73.6	71.4	47.0	49.1	50.1	54.2	9.2	10.3	38.0	0.03691
12	2041.7	91.7	47.3	47.7	97.7	93.7	114.6	118.0	128.6	125.1	125.1	121.8	150.8	123.9	132.1	133.4	56.0	64.9	64.1	62.3	45.3	46.9	47.8	51.4	9.4	10.5	35.7	0.04171
13	1860.8	90.8	44.5	44.4	80.8	79.4	91.9	92.3	104.4	101.0	100.6	97.4	124.5	99.1	105.2	105.4	45.8	54.8	54.5	51.7	43.1	44.6	45.0	48.1	9.5	10.7	35.7	0.04511
14	1652.9	88.9	41.1	41.0	63.4	62.3	68.1	66.0	77.5	74.6	73.2	70.7	92.5	69.8	72.2	72.3	36.6	44.8	44.4	42.3	40.3	41.2	41.6	44.7	9.7	10.7	35.7	0.07602
15	1250.6	90.2	36.0	35.9	50.5	49.1	54.5	57.6	68.5	62.3	55.9	54.5	71.2	53.5	53.2	53.3	31.8	39.7	39.4	37.3	35.2	36.1	36.0	39.1	9.0	10.0	37.4	0.06861
16	1049.5	90.0	32.7	32.6	46.6	44.7	49.9	50.3	61.2	57.8	52.0	50.6	69.0	53.5	51.5	50.5	30.2	36.9	37.1	34.5	31.3	32.7	33.2	35.2	8.5	9.7	37.3	0.05911
17	851.5	89.6	30.4	30.3	43.2	41.4	46.5	48.1	56.7	53.3	48.0	47.3	62.2	49.5	49.8	48.8	27.5	34.7	34.9	32.8	29.7	30.5	30.9	33.0	9.2	10.5	34.5	0.05570
18	649.8	90.6	27.6	28.1	39.3	36.9	42.0	43.1	51.6	48.8	43.6	43.4	54.9	45.0	45.3	44.8	24.2	32.4	32.0	30.0	26.9	28.8	28.1	30.2	9.2	10.5	31.6	0.06350
19	450.6	90.4	24.8	24.1	33.7	31.4	35.7	38.6	44.4	43.8	38.5	38.4	46.0	38.3	40.3	40.4	21.0	29.1	28.7	26.1	23.5	24.8	24.8	27.4	10.1	10.7	34.5	0.04040
20	249.0	90.0	20.3	20.0	25.8	24.3	28.4	30.8	33.7	33.7	33.0	32.3	34.2	39.8	31.4	31.4	16.2	24.1	23.6	21.1	19.6	20.3	20.3	22.9	9.5	10.3	35.8	0.03510

Table A1-4: Steady state data for VHVC orientation

Sr. No.	Power (W)	PI-1	T-17 (°C)	T-18 (°C)	T-19 (°C)	T-20 (°C)	T-21 (°C)	T-22 (°C)	T-23 (°C)	T-24 (°C)	T-25 (°C)	T-26 (°C)	T-27 (°C)	T-28 (°C)	T-29 (°C)	T-30 (°C)	T-31 (°C)	T-32 (°C)	T-33 (°C)	T-34 (°C)	T37 (°C)	T38 (°C)	T39 (°C)	T40 (°C)	T-43 (°C)	T-44 (°C)	LPM	Mass flow rate
1	601.9	81.8	25.3	25.8	39.3	35.8	41.4	44.2	42.1	41.5	42.5	41.2	46.0	40.5	41.4	43.2	26.4	30.8	30.9	28.4	30.9	30.2	25.3	22.1	8.9	9.1	36.2	0.03626
2	995.6	81.6	32.1	32.0	48.8	45.8	52.8	53.7	58.4	55.5	55.9	54.0	67.8	52.9	54.3	55.5	30.7	35.2	35.4	32.8	36.0	35.2	32.0	28.7	8.9	9.3	36.2	0.04537
3	904.0	81.8	31.0	31.4	47.2	45.2	51.1	50.3	55.0	52.7	52.5	51.2	63.3	49.5	50.9	53.3	30.2	35.2	34.9	32.8	35.4	35.2	31.5	28.1	9.3	9.7	36.2	0.03846
4	699.8	81.4	28.7	29.2	42.1	39.1	44.8	44.8	47.7	45.4	45.8	44.5	55.5	45.0	45.3	47.1	29.1	33.0	33.2	31.2	33.8	33.0	29.2	25.4	9.3	9.5	36.6	0.0392
5	499.7	81.4	25.3	25.8	37.6	34.7	39.7	39.7	41.5	39.8	40.2	40.1	47.1	39.4	40.3	41.5	32.3	30.2	30.4	28.4	30.4	30.2	25.3	22.1	9.0	9.3	38.3	0.03256
6	299.9	81.4	22.0	21.9	30.9	28.1	34.0	33.0	35.0	33.7	35.2	34.5	39.2	34.3	35.3	35.9	28.6	25.7	25.9	23.9	26.4	26.3	21.9	17.6	8.9	9.0	38.3	0.03101
7	102.3	80.4	17.5	17.4	21.3	19.3	23.8	22.4	24.1	24.1	24.6	23.9	25.8	24.8	24.1	25.8	23.2	20.1	20.2	18.4	21.4	21.2	16.9	13.2	8.8	9.0	38.3	0.01992
8	202.5	81.2	19.1	19.1	25.8	23.7	28.9	27.4	29.8	28.6	30.2	29.5	32.0	29.3	30.2	31.4	25.3	22.9	23.0	21.1	23.6	22.9	18.5	15.4	9.3	9.3	38.2	0.02251
9	405.5	81.1	23.1	23.0	33.7	31.4	36.9	38.6	38.2	37.0	37.4	36.7	43.2	37.2	38.6	38.7	31.2	28.0	27.5	25.6	28.1	28.5	23.0	19.3	9.3	9.5	37.8	0.03314
10	594.8	80.4	27.0	26.9	38.7	36.4	41.4	42.5	43.8	42.1	41.9	41.2	49.9	41.1	41.4	43.2	30.2	31.3	31.5	29.5	31.5	31.9	27.0	23.7	9.2	9.5	54.8	0.03692
11	205.8	84.6	19.1	19.6	26.4	23.7	29.5	27.4	29.8	29.2	30.2	30.0	32.5	29.8	30.2	32.0	17.8	22.9	23.6	20.6	24.2	24.0	19.4	14.9	9.3	9.3	51.3	0.02608
12	421.2	84.3	22.0	21.9	33.7	31.4	36.9	31.9	38.2	37.6	37.4	37.3	43.7	36.6	38.1	38.7	22.1	26.9	27.0	24.5	27.6	26.8	21.3	18.2	8.8	9.0	54.0	0.03439
13	583.5	85.6	24.7	24.8	38.7	36.4	42.0	37.5	43.8	42.1	41.9	41.2	50.5	41.1	42.0	43.2	25.3	30.2	30.4	28.4	30.4	30.2	25.3	21.5	8.7	8.8	54.4	0.03532
14	809.0	85.4	28.7	28.6	44.4	41.9	47.7	44.8	51.1	48.2	48.6	47.8	58.9	46.7	48.1	49.3	28.6	33.0	33.7	31.7	33.5	34.3	28.7	24.8	8.9	9.0	54.4	0.04488
15	1017.6	85.2	31.5	30.9	50.5	47.4	54.5	50.9	58.4	55.5	55.9	54.5	68.4	53.5	54.9	56.1	30.2	35.8	35.4	33.4	36.0	35.8	31.5	28.1	8.7	9.0	54.4	0.05612
16	1635.5	85.0	37.2	37.6	88.1	85.5	79.4	76.6	93.8	89.8	90.5	88.8	103.7	81.1	81.7	82.4	36.1	40.8	41.0	38.9	41.6	41.4	37.6	33.6	9.2	9.4	56.0	0.0449
17	1803.7	85.0	38.3	38.7	111.2	109.7	94.8	95.7	116.2	112.2	114.5	111.8	130.1	105.8	110.3	112.7	43.1	49.2	48.9	46.7	48.9	49.2	38.8	34.7	9.2	9.6	55.3	0.03095
18	1999.6	84.8	41.1	41.5	151.0	148.3	127.1	125.3	158.3	154.8	160.3	157.4	178.8	154.8	164.0	167.6	63.0	68.8	68.0	65.6	66.9	66.5	41.6	37.5	9.3	9.5	55.6	0.02666
19	1899.5	86.0	40.5	40.4	128.6	126.3	107.8	106.9	134.7	131.3	134.1	131.8	150.2	126.7	133.2	135.7	52.3	58.2	57.3	55.1	57.4	57.0	41.0	36.9	9.3	9.7	55.6	0.0304
20	1509.5	85.4	37.7	37.6	83.1	81.0	76.0	761.0	93.2	89.8	89.9	87.9	100.9	79.4	80.1	81.3	36.6	41.4	41.6	39.5	42.2	41.9	38.2	34.2	9.0	9.5	46.2	0.04047
21	1205.6	85.2	33.2	33.1	56.7	54.6	59.6	57.6	65.1	62.3	63.1	61.2	76.8	59.1	61.0	62.2	31.8	36.9	36.5	34.5	37.1	36.9	33.7	29.8	9.0	9.2	55.8	0.0711
22	905.3	84.1	31.1	31.4	47.7	45.2	50.5	51.5	55.0	52.2	52.5	50.6	63.3	49.5	51.5	51.6	28.0	34.7	34.9	32.3	35.4	34.7	30.9	27.6	9.3	9.5	46.3	0.06186
23	499.3	85.2	25.9	25.8	33.1	31.4	35.7	31.9	37.1	35.9	38.0	37.3	45.4	37.7	38.6	39.8	56.6	30.2	30.4	28.4	30.4	30.2	25.8	22.1	9.4	9.5	46.2	0.03839
24	200.6	89.9	19.7	19.6	24.1	21.5	25.0	23.5	26.4	25.8	26.3	25.6	29.2	25.9	26.3	27.5	90.0	22.9	23.6	21.7	24.2	24.0	19.1	16.0	9.5	9.5	37.9	0.02377
25	507.6	88.7	23.6	23.0	37.1	34.7	40.9	42.5	42.7	41.5	41.9	41.2	48.8	40.5	42.0	42.6	83.0	29.1	29.8	26.7	29.8	29.1	23.0	19.8	8.8	9.0	46.0	0.03113
26	995.9	90.4	31.5	32.8	54.6	49.1	55.6	57.1	60.1	57.8	57.5	55.6	70.1	54.6	56.5	58.3	94.3	37.5	37.7	35.6	37.7	37.5	31.5	28.1	8.6	8.9	46.1	0.0407